Treball de Final de Grau en Enginyeria Física

Quantum Many-Body Systems in 1D: One Dimensional Hydrogen.

Alfredo José Vidal Arias

Advisors: Grigori Astrakharchik and Jordi Boronat

June 22, 2015

Contents

Abstract

The ground-state properties of one-dimensional spin polarized ^{1}H, ^{2}H and ^{3}H at zero temperature are obtained by means of Diffusion Monte Carlo calculations. The equations of state of the three isotopes are found and compared in a wide range of densities, understanding its limits at low and high densities. The pair correlation function and the static structure factor are computed and also interpreted within the frame work of Luttinger liquid theory. The Luttinger parameter is explicitly found, from which we can identify different physical regimes, among which are: 'Fermi gas', 'Bose-gas', 'super-Tonks-Girardeau' and 'quasi-crystal' regime. The role of the mass in the system behaviour is found to be a non-straightforward one, finding remarkable differences between tritium and the other two isotopes at low densities.

1. *Introduction*

The interest on ultra-cold quantum gases has greatly increased since the achievement and observation of Bose-Einstein condensate (BEC) of ^{87}Rb in 1995 by Eric Cornell and Carl Wieman [1], many years after the theoretical foundations of the Bose-Einstein statistics were stated by Satyendranath Bose [2] and Albert Einstein [3, 4], and Fermi-Dirac statistics by Paul Dirac [5] and Enrico Fermi [6]. Since then, the technical improvements in cooling down to near zero-temperature and confining atoms have allowed to realize BEC in different isotopes like ^{4}He, ^{41}K, molecules, quasi-particles and photons [7], and have motivated a theoretical interest and work in the field.

The possibility of cooling down gases to near zero-temperature, the actual minimum being of a half of a billionth Kelvin reached by MIT [8] in 2003, and the improvement in techniques for confining atoms to low-dimensional geometries [9, 10, 11, 12], have enabled the experimental study of these systems, obtaining characteristic quantities like the energy, momentum distribution, static structure factor, etc. Low-dimensional systems have remarkable differences respect to the three dimensional ones, emerging non-straightforward behaviours like the absence of Bose condensation in the one dimensional case or the *fermionization* of bosons described by the Luttinger theory [13], which provides a theoretical background to the study accomplished in this work.

Hydrogen is the simplest atom and it is of fundamental interest to study its properties. The interatomic potential of spin polarized hydrogen $H_\downarrow - H_\downarrow$ has been previously obtained almost exactly in different works by Kolos, Jamieson, Dalgarno and Wolniewicz[14, 15, 16] enabling further studies on systems of hydrogen and its isotopes deuterium and tritium, in which the effective potential is the same, regardless the mass. This knowledge has made possible to perform different studies of the properties of hydrogen isotopes at low temperatures [17, 18, 19, 20]. Altough there is yet no experimental realization of 1D hydrogen due to technical difficulties, unlike achievements with other atoms such as ^{3}He [21], the study of hydrogen involving low-dimensional geometry in which the role of quantum fluctuations is further increased has a large fundamental and experimental importance. Up to now, only the case of the para-hydrogen was studied in Ref.[22]

The numerical techniques employed to study quantum many-body systems have been developed during the last century, Monte Carlo methods [23] being the most efficient ones carrying out a multidimensional integration of $3N$ degrees of freedom (for the 3-dimensional case). Most of Monte Carlo methods are able of solving and finding the zero-temperature ground-state properties. Diffusion Monte Carlo (DMC) and the reptation Monte Carlo (RMC) are methods that solve the ground state. For instance, the Path Integral Monte Carlo is used for finite temperature. In our case, the diffusion Monte Carlo method (DMC) is the most

suitable for our study, and is the one we have implemented jointly to the Variational Monte Carlo (VMC).

Objectives

The final goal of the work is the detailed characterization of one-dimensional spin-polarized hydrogen together with its isotopes: deuterium and tritium. We aim to calculate the equation of state (the energy in terms of the density), the pair correlation function and the static structure factor, and also to extract the Luttinger parameter dependence on the linear density. It is also among the objectives to differentiate the main regimes exhibited by the system from ideal Fermi gas IFG to quasi-crystal. We will demonstrate that the physical behaviour of the system at low densities is related to that of the IFG and hard-rod gas models, while at high densities the system properties can be interpreted in terms of the classical harmonic crystal model.

Outline of the work

The work here presented is organized in the following way:

- In the second chapter called “Theoretical background” some general theoretical background relevant for the work and different approaches that will be employed are presented.
- In Chapter 3 ”Methods and tools” the Monte Carlo methods implemented are shortly explained, as well as the definitions and details of the magnitudes that are going to be measured, and also an few words on the error estimation.
- In Chapter 4 ”One-dimensional Hydrogen” we discuss the specific aspects related to our problem. We provide details on the hydrogen interaction potential and the guiding wave function, including the definitions of the parameters related to it or the numerical solution of the scattering problem.
- In Chapter 5 the results obtained with both methods VMC and DMC are show, paying particular attention to the DMC ones; the equation of state, the static structure factor, the pair correlation function and the Luttinger parameter are presented.
- Finally the conclusions of the work are drawn in the Chapter 6. At the end the bibliography is added.
- The Annex contains a test of the DMC code. We analyse its performance with the quantum harmonic oscillator.

2. *Theoretical background*

In this Chapter we will pose the many-body quantum problem, we will review the two-body scattering problem and a set of models for one-dimensional quantum gases. We will review crystal properties in one dimension. Concepts that can be helpful in solving and understanding the results of the one-dimensional hydrogen system will also be discussed.

2.1 Quantum Many-Body problem

In principle the quantum state of a system can be described by means of the Schrödinger equation and so all the relevant information is contained in the wave function $|\Psi(t)\rangle$ associated with the system state.

The Schrödinger equation can be written for its time-dependent version in the following way

$$\hat{\mathcal{H}} |\Psi(t)\rangle = i\hbar \frac{\partial}{\partial t} |\Psi(t)\rangle \tag{2.1}$$

where the Hamiltonian is a sum of kinetic and potential energy parts $\hat{\mathcal{H}} = \hat{T} + \hat{V}$. The time-independent version, true for all stationary states and therefore for all the eigenvectors or eigenstates of the Hamiltonian, can be written

$$\hat{\mathcal{H}} |\Psi_n\rangle = \epsilon_n |\Psi_n\rangle , \qquad \text{where} \qquad |\Psi_n(t)\rangle = e^{-\frac{i}{\hbar}\epsilon_n t} |\Psi_n(0)\rangle \tag{2.2}$$

where the wave function $|\Psi\rangle$ belongs to a certain Hilbert space of a dimension given by the degrees of freedom and the number of particles.

The Hamiltonian for a system of N particles can be written in terms of the kinetic energy and potential energy operators

$$\hat{\mathcal{H}} = \sum_{i=1}^{N} \hat{T}_i + \hat{V} = \sum_{i=1}^{N} \frac{\hat{p}_i \cdot \hat{p}_i}{2m_i} + \hat{V} = -\sum_{i=1}^{N} \frac{\hbar^2}{2m_i} \Delta_i + V(\hat{r}_1, \ldots, \hat{r}_N, t) \tag{2.3}$$

where the potential energy includes on the interaction between the particles and the external fields, and moreover can be time-dependent.

For example, in order to model a system of few atoms a model can be considered where the interaction of nuclei and electrons are taken into account explicitly through Coulomb potential

$$\hat{\mathcal{H}} = -\sum_i \frac{\hbar^2}{2m_e}\Delta_i - \sum_n \frac{\hbar^2}{2M}\Delta_n + \frac{e^2}{4\pi\epsilon_0}\left(\frac{1}{2}\sum_{i<j}\frac{1}{|\hat{r}_i - \hat{r}_j|} - \sum_{i,n}\frac{Z_n}{\left|\hat{r}_i - \hat{R}_n\right|} + \frac{1}{2}\sum_{n<m}\frac{Z_n Z_m}{\left|\hat{R}_n - \hat{R}_m\right|}\right) \tag{2.4}$$

By ignoring the internal structure, atoms can be treated as composite particles replacing the Coulomb potential with the effective interaction potential between atoms, provided it is known, resulting in

$$\hat{\mathcal{H}} = \frac{\hbar^2}{2m}\sum_i \Delta_i + \sum_{i<j} V_{eff}\left(|\hat{r}_i - \hat{r}_j|\right) \tag{2.5}$$

2.2 Two-body scattering problem

The scattering problem of two (and three bodies) is helpful once we want to approximate the wave function of a many-body system at short inter-particle distances and in diluted systems. So here we will approach the two-body scattering problem and we will discuss its properties for short-range potentials.

Let us consider a generic two-particle Hamiltonian

$$\hat{\mathcal{H}} = \frac{\hat{p}_1 \cdot \hat{p}_1}{2m_1} + \frac{\hat{p}_2 \cdot \hat{p}_2}{2m_2} + V\left(|\hat{r}_1 - \hat{r}_2|\right) = -\frac{\hbar^2}{2m_1}\Delta_1 - \frac{\hbar^2}{2m_2}\Delta_2 + V\left(|\hat{r}_1 - \hat{r}_2|\right) \tag{2.6}$$

One can decouple the dynamics of the center of mass and relative coordinate, as is done in the classical mechanics problem. We define

$$R = \frac{m_1 r_1 + m_2 r_2}{m_1 + m_2} \qquad r = r_1 - r_2 \qquad \mu = \frac{m_1 m_2}{m_1 + m_2} \qquad M = m_1 + m_2 \tag{2.7}$$

where R is the coordinate for the center of mass (CM), r is the relative coordinate, μ is the reduced mass (it is the effective inertial mass) and M is the total mass of the system. From this change of coordinates we can infer the new momentum operators, from the expression of the Laplacian

$$\Delta_i = \left(\frac{\partial R}{\partial r_i}\right)^2 \frac{\partial^2}{\partial R^2} + \left(\frac{\partial R}{\partial r_i}\frac{\partial r}{\partial r_i}\right)\left(\frac{\partial^2}{\partial r \partial R} + \frac{\partial^2}{\partial R \partial r}\right) + \left(\frac{\partial r}{\partial r_i}\right)^2 \frac{\partial^2}{\partial r^2} \tag{2.8}$$

then

$$\begin{aligned} \Delta_1 &= \left(\frac{\mu}{m_2}\right)^2 \Delta_R + \left(\frac{\mu}{m_2}\right)\left(\frac{\partial^2}{\partial r \partial R} + \frac{\partial^2}{\partial R \partial r}\right) + \Delta_r \\ \Delta_2 &= \left(\frac{\mu}{m_1}\right)^2 \Delta_R - \left(\frac{\mu}{m_1}\right)\left(\frac{\partial^2}{\partial r \partial R} + \frac{\partial^2}{\partial R \partial r}\right) + \Delta_r \end{aligned} \tag{2.9}$$

and so the Hamiltonian can be written as

$$\hat{\mathcal{H}} = \frac{\hat{p}_R \cdot \hat{p}_R}{2M} + \frac{\hat{p}_r \cdot \hat{p}_r}{2\mu} + V\left(|\hat{r}|\right) = -\frac{\hbar^2}{2M}\Delta_R - \frac{\hbar^2}{2\mu}\Delta_r + V\left(|\hat{r}|\right) \tag{2.10}$$

Therefore the Schrödinger equation gets separated in the center of mass part and the relative coordinate part. Assuming $\Psi = \Psi_R \Psi_r$ we find that

$$\epsilon + \frac{\hbar^2}{2M}\frac{\Psi_R''}{\Psi_R} = -\frac{\hbar^2}{2\mu}\frac{\Psi_r''}{\Psi_r} + V(|r|) \tag{2.11}$$

and therefore

$$\begin{aligned} \epsilon_r \Psi_r &= -\frac{\hbar^2}{2\mu}\Delta_r \Psi_r + V\left(|r|\right)\Psi_r \\ \epsilon_R \Psi_R &= -\frac{\hbar^2}{2M}\Delta_r \Psi_R \end{aligned} \tag{2.12}$$

where the total energy is $\epsilon = \epsilon_r + \epsilon_R$. When we reduce the dimensionality of our problem to 1D the Schrödinger equation, in which we are interested, and get

$$\begin{aligned} \epsilon_r \Psi_r &= -\frac{\hbar^2}{2\mu}\Psi_r'' + V\left(|r|\right)\Psi_r \\ \epsilon_R \Psi_R &= -\frac{\hbar^2}{2M}\Psi_R'' \Longrightarrow \Psi_R = e^{iK_R R} \quad \text{where} \quad k_r = \sqrt{\frac{2M\epsilon_R}{\hbar^2}} \end{aligned} \tag{2.13}$$

and hence the solution in 1D can be written as the product of a plane wave for the center of mass part and the solution of relative coordinate. It is convenient to write the relative motion Schrodinger equation in terms of the scattering momentum $k^2 = \frac{\epsilon_r 2\mu}{\hbar^2}$

$$\Psi_r'' = -\left(k^2 - \frac{2\mu}{\hbar^2}V\left(|r|\right)\right)\Psi_r \tag{2.14}$$

For distances much larger than the range of the potential the solution takes form of a plane wave

$$\Psi_r(r) = A\cos\left(k|r| - \delta(k)\right) \tag{2.15}$$

where $\delta(k)$ is called the *scattering phase* and defines the one-dimensional scattering length for the limit of low energy

$$a_{1\mathrm{D}} = -\lim_{k\to 0}\frac{\partial\delta(k)}{\partial k} \tag{2.16}$$

It is expected that in the weakly-interacting regime the system properties depend on a single parameter only, namely the s-wave scattering length $a_{1\mathrm{D}}$.

We are interested in studying the low-energy solution for two particular models, the hard-rod and the pseudo-potential ones.

2.2.1 Hard rod potential

It is a common feature of realistic inter-atomic potentials to posses a hard core for short distances. We will consider a hard-core potential of the form

$$V(|r|) = \begin{cases} \infty & 0 < |r| < a_{1\mathrm{D}} \\ 0 & \infty > |r| > a_{1\mathrm{D}} \end{cases} \tag{2.17}$$

where the diameter of the hard rod $a_{1\mathrm{D}}$ coincides with the scattering lenght defined previously in equation (2.16).

Then for $|r| < a_{1D}$ there is a zero probability of finding two particles and the solution is $\Psi(r) = 0$. For $|r| > a_{1\mathrm{D}}$ the problem reduces to a free-scattering

$$\Psi_r^{''} = -k^2 \Psi_r \tag{2.18}$$

with the solution given by a plane wave

$$\Psi_r(r) = A \sin\left[k(|r| - a_{1\mathrm{D}})\right] \qquad r > a_{1\mathrm{D}} \tag{2.19}$$

we impose boundary conditions at $r = L/2$ and so A is a normalization constant given by

$$A^2 = \left(\int_{-L/2}^{L/2} \Psi_r^2(r) dr \right)^{-1} \tag{2.20}$$

and k is fixed in order to fulfill the boundary conditions at $r = \pm \frac{L}{2}$

$$\Psi_r^{'}\left(\frac{L}{2}\right) = -\Psi_r^{'}\left(-\frac{L}{2}\right) \Longrightarrow \cos\left[k\left(\frac{L}{2} - a_{1\mathrm{D}}\right)\right] = 0 \Longrightarrow k = \frac{(2n+1)\,\pi}{2\left(\frac{L}{2} - a_{1\mathrm{D}}\right)} \tag{2.21}$$

In summary, the s-wave scattering solution for the hard-rod potential is

$$\Psi_r(r) = k \csc\left[k\left(a - \frac{L}{2}\right)\right] \sin\left[k(|r| - a_{1\mathrm{D}})\right] \theta\left(|r| - a_{1\mathrm{D}}\right) \qquad k = \frac{(2n+1)\,\pi}{2\left(\frac{L}{2} - a_{1\mathrm{D}}\right)} \tag{2.22}$$

2.2.2 1D Pseudopotential

It is usual to approximate the inter-atomic potential with a pseudo-potential when considering ultra cold quantum gases. We assume a potential of the form of a contact pseudo-potential

$$V(r) = g\delta(r) \tag{2.23}$$

where g is the coupling constant. We can relate the coupling constant to the scattering length in the following way

$$-\frac{\hbar^2}{2\mu}\Psi_r^{''} + g\delta(r)\Psi_r = \epsilon_r \Psi_r \Longrightarrow \lim_{\epsilon \to 0} \int_{-\epsilon}^{\epsilon} -\frac{\hbar^2}{2\mu}\Psi_r^{''}(r) + g\delta(r)\Psi_r(r) dr = \epsilon_r \lim_{\epsilon \to 0} \int_{-\epsilon}^{\epsilon} \Psi_r(r) dr \tag{2.24}$$

$$-\frac{\hbar^2}{\mu}\Psi_r^{'}(0)+g\Psi_r(0)=0\Longrightarrow g=\frac{\hbar^2}{\mu}\left.\frac{\Psi_r^{'}}{\Psi_r}\right|_{r=0} \tag{2.25}$$

that can be related to the previous model for the zero-energy scattering approximation $k\to 0$, obtaining

$$\begin{aligned}\lim_{k\to 0}\left.\frac{\Psi_{HR}^{'}}{\Psi_{HR}}\right|_{r=0}&=\lim_{k\to 0}\left.\frac{Ak\cos\left(k\left(|r|-a_{1D}\right)\right)}{A\sin\left(k\left(|r|-a_{1D}\right)\right)}\right|_{r=0}=\lim_{k\to 0}\left.\frac{k}{\tan\left(k\left(|r|-a_{1D}\right)\right)}\right|_{r=0}=\\&=\left.\frac{1}{|r|-a_{1D}}\right|_{r=0}=-\frac{1}{a_{1D}}\end{aligned} \tag{2.26}$$

then

$$g=-\frac{\hbar^2}{a_{1D}\mu} \tag{2.27}$$

In practical, for scattering of two equal particles, $m_1=m_2$, the coupling constant g is related to the s-wave scattering length $a_{1\mathrm{D}}$ as

$$g=-\frac{2\hbar^2}{ma_{1\mathrm{D}}} \tag{2.28}$$

2.2.3 Different behaviours in 1D

From the two toy-model potentials we have analysed above we can deduce four main behaviours in one dimensional systems. If $g>0$ and consequently $a_{1D}<0$ we have a repulsive system and no bound states. When $g<0$ and $a_{1D}>0$ the system is in a bound state. For $g\to 0$ and so $|a_{1D}|\to\infty$ there is no interaction so the resulting wave function is the same as that of the free wave. In the case of $g\to+\infty$ and then $a_{1D}\to 0$ the state is in the called Tonks-Girardeau regime, equivalent to a hard rod potential with $a_{1\mathrm{D}}=0$, where the particles in the gas behave like a point-like impenetrable bosons. If $g\to-\infty$, it is large and negative a different gas state appears, called super Tonks-Girardeau [24], where the correlations in the gas are stronger and the hard core becomes non-punctual.

2.3 Tonks-Girardeau. Ideal Fermi gas

As we mentioned above, Tonks-Girardeau is one of the interesting limits for quantum gases, in which particles interact in terms of an infinitely strong delta function, becoming impenetrable point-particle objects. The wave function of this kind of gas can be mapped to that of an ideal Fermi gas (IFG). We can describe a non-interacting gas of fermions in a box of size L by means of a Hamiltonian which takes into account only the kinetic term.

$$\left(-\frac{\hbar^2}{2m}\sum_{i=1}^{N}\nabla_i^2\right)\Psi\left(r_1,r_2,\dots r_N\right)=E\Psi\left(r_1,r_2,\dots r_N\right) \tag{2.29}$$

Such a model can be solved by means of the Slater determinant of a set of base functions. In the case of a homogeneous system, the base consists of plane waves $\phi(x_j) = e^{i\frac{2\pi}{L}x_j}$. Solving the problem in one dimension one finds

$$\Psi_F(x_1,\ldots,x_N) \propto \begin{vmatrix} \phi^0(x_1) & \cdots & \phi^{N-1}(x_1) \\ \vdots & \ddots & \vdots \\ \phi^0(x_N) & \cdots & \phi^{N-1}(x_N) \end{vmatrix} \qquad \text{where} \tag{2.30}$$

where the momentum is discretized according to periodic boundary conditions, $k = \frac{2\pi n}{L}$ with $n \in \mathbb{N}$, and the energy $\epsilon = \frac{\hbar^2 k^2}{2m}$. In one dimension the Slater determinant can be written as a Vandermonde determinant and can be explicitly evaluated resulting in a pair product

$$\Psi_F(x_1,\ldots,n_N) \propto \prod_{i<j}^{N} [\phi(x_i) - \phi(x_j)] = \prod_{i<j}^{N} \left(e^{i\frac{2\pi}{L}x_i} - e^{i\frac{2\pi}{L}x_j}\right) = 2i \prod_{i<j}^{N} e^{i\frac{\pi}{L}(x_i+x_j)} \sin\left[\frac{\pi}{L}(x_i - x_j)\right] \tag{2.31}$$

According to Girardeau's mapping for point-like impenetrable Bosons $\Psi_B = |\Psi_F|$ [25]

$$\Psi_B(x_1,\ldots,n_N) \propto \prod_{i<j}^{N} \left|\sin\left[\frac{\pi}{L}(x_i - x_j)\right]\right| \tag{2.32}$$

We will find the ground-state energy as it is an important quantity characterizing the system. First of all we note that the energy of the level with momentum $k = \frac{2\pi n}{L}$ has the energy

$$\epsilon = \frac{\hbar^2 k^2}{2m} \qquad \text{and} \qquad k = \frac{2\pi}{L} n \tag{2.33}$$

An important momentum scale is associated with the last energy level occupied, is the Fermi momentum k_F. In terms of the number of particles, for the degenerate case ($T = 0K$) in one dimension one has

$$N = \sum_j n(k_j) = \frac{L}{2\pi} \int_{-\infty}^{\infty} n(k)dk = \frac{L}{2\pi} \int_{-k_F}^{k_F} n(k)dk \Longrightarrow k_F = \frac{N\pi}{L} = \pi\rho \tag{2.34}$$

That is in 1D the Fermi momentum is linear in density. The chemical potential is the energy at the Fermi level

$$\mu = E_F = \epsilon(k_F) = \frac{\hbar^2 k_F^2}{2m} = \frac{\hbar^2 \pi^2 \rho^2}{2m} \tag{2.35}$$

and is quadratic in density. The energy per particle is obtained by the integrating the chemical potential

$$\frac{E}{N} = \frac{1}{N} \int_0^N \mu(N)dN = \frac{\pi^2 \hbar^2 \rho^2}{6m} \tag{2.36}$$

There are no other energy and momentum scales than E_F and k_F. In therms of velocity the relevant scale is the Fermi velocity

$$v_F = \frac{p_F}{m} = \frac{\sqrt{2m\epsilon_F}}{m} = \frac{\sqrt{2m\frac{\hbar^2\pi^2\rho^2}{2m}}}{m} = \frac{\hbar\pi}{m}\rho \tag{2.37}$$

From the thermodynamic definition of the speed of sound in an homogeneous media

$$c = \sqrt{-\frac{1}{m}\left(\frac{\partial P}{\partial \rho}\right)_N} \qquad \text{and} \qquad P = -\left(\frac{\partial E}{\partial L}\right)_N \tag{2.38}$$

we can see that, indeed, the speed of sound in an TG/IFG is given by the Fermi velocity.

$$P = \frac{\pi^2\hbar^2}{3m}\rho^3 \qquad \Longrightarrow \qquad c = \frac{\pi\hbar}{m}\rho = v_{\mathrm{F}} \tag{2.39}$$

We can also calculate the static structure factor of TG/IFG at zero temperature. The degenerated IFG presents a momentum distribution of the form $n_k = \Theta\left(|k_F - k|\right)$, it is the particles are distributed uniformly along the momentums up to k_F. Then we can compute

$$\begin{aligned} S_q &= \frac{1}{N}\sum_k n_k\left(1 - n_{k+q}\right) = \frac{1}{2k_F}\int_{-\infty}^{\infty} n_k\left(1 - n_{k+q}\right)dk = \\ &= \frac{1}{2k_F}\int_{-\infty}^{\infty} \Theta\left(|k_F - k|\right)\left[1 - \Theta\left(|k_F - k - q|\right)\right]dk = \\ &= \Theta\left(q - 2k_F\right) + \frac{q}{2k_F}\left(\Pi\left[\frac{q}{2k_F} - \frac{1}{2}\right]\right) \end{aligned} \tag{2.40}$$

And furthermore find the correlation function $g(r)$ related to the inverse Fourier transform of S_q, then the pair distribution function is

$$\begin{aligned} g(r) &= 1 - \left|\frac{1}{L}\sum_k n_k e^{ikr}\right|^2 = 1 - \left|\frac{1}{2k_F}\int_{-\infty}^{\infty}\Theta\left(|k_F - k|\right)e^{ikr}dk\right|^2 = \\ &= 1 - \left(\frac{\sin\left(k_F x\right)}{k_F x}\right)^2 = 1 - \mathrm{sinc}^2\left(k_F x\right) \end{aligned} \tag{2.41}$$

where the functions $\Theta(x)$ and $\Pi(x)$ are defined below

$$\Theta(x) = \begin{cases} 1 & x > 0 \\ 0 & x < 0 \end{cases} \qquad \text{and} \qquad \Pi(x) = \begin{cases} 1 & |x| < \dfrac{1}{2} \\ 0 & |x| > \dfrac{1}{2} \end{cases} \tag{2.42}$$

It can be shown that the pair correlation function and the Static structure factor of an TG gas are the same as that of the IFG, however we have to notice that the momentum distribution is not equivalent

2.3.1 Hard-rod gas

We can think in a hard-rod gas as a variation of the TG gas where the size of the box is reduced by the 'excluded volume', which is proportional to the number of particles, so in this case, the energy per particle becomes

$$\frac{E}{N} = \frac{\pi^2\hbar^2}{6m}\frac{N^2}{(L - a_{1D}N)^2} = \frac{\pi^2\hbar^2}{6m}\frac{\rho^2}{(1 - \rho a_{1D})^2} \tag{2.43}$$

For small $a_{1\mathrm{D}}$ Eq. (2.43) can be seen as a correction to TG gas energy

$$\frac{E}{N} = \frac{\pi^2\hbar^2}{6m}\left(\rho^2 + 2a_{1D}\rho^3 + \cdots\right) \tag{2.44}$$

2.4 Gross–Pitaevskii gas

The Gross-Pitaevskii equation describes the ground state of a bosonic quantum system within the Hartree-Fock and the first Born approximations. When all particles are Bose-condensed, the wave function of the system follows the Gross Pitaevskii equation

$$\left(-\frac{\hbar^2}{2m}\frac{\partial^2}{\partial x^2} + V(x) + \frac{1}{2}g\left|\psi(x)\right|^2\right)\psi(x) = \mu\psi(x) \qquad \text{where} \qquad g = \frac{4\pi\hbar^2 a_s}{m} \tag{2.45}$$

and where the normalization condition

$$N = \int \left|\psi(x)\right|^2 dx \tag{2.46}$$

defines implicitely the chemical potential μ. In the simplest case, if $V(x) = 0 \quad |x| < L/2$ in a box, we can find the solution of the nonlinear equation is

$$\psi(x) = \sqrt{\rho}e^{ikx} \qquad \rho = N/L \tag{2.47}$$

where $\mu = \frac{\hbar^2}{2m}k^2 + g\rho$ and so the energy per particle of the system

$$\frac{E}{N} = \frac{1}{N}\int_0^N \mu(N)dN = \frac{\hbar^2k^2}{2m} + \frac{1}{2}g\rho \tag{2.48}$$

that is minimum for $k = 0$, being

$$\frac{E}{N} = \frac{1}{2}g\rho \tag{2.49}$$

To summarize, within the mean field approximation, the chemical potential and the energy per particle are linear in density.

2.5 High density limit. Ideal crystal

The previous models of quantum gases can be found as a certain limits for low densities in real gases (like in our case). We are also interested in finding a suitable fit for large densities if possible, mainly in the description of the energy. The first approach is to consider the ideal

crystal, it is all the atoms perfectly localized at the equilibrium position $x_i = a \cdot i$, where $a = 1/\rho$, and so

$$\frac{E_{IC}}{N} = \sum_{n=1}^{\infty} V(an) \tag{2.50}$$

However this approach may not be enough accurate since atoms can move around the minimum energy position, and a second order would be convenient. Lets imagine an unidimensional mono-atomic solid, and assume that the potential is well approximated by an harmonic potential, it is the approximation of harmonic potential, valid for small movement of the crystal atom around the equilibrium point. Lets also assume periodic boundary conditions.

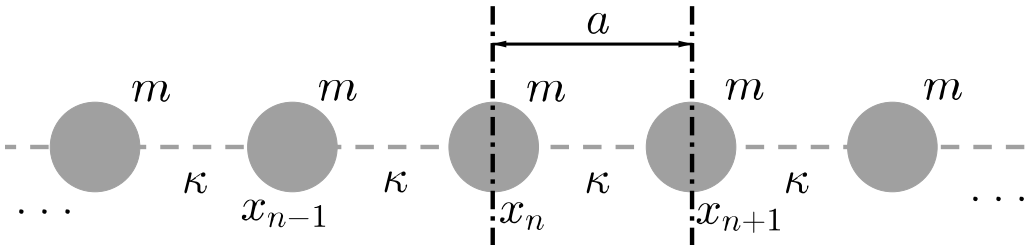

Figure 2.1: One-dimensional ideal crystal

We want to compute the energy of the crystal, but we must find the frequency of an elastic wave (phonon) going through the crystal, in terms of the wave vector k. From the classical equations of motion for each atom we have the eigenvalue equation of interest. For the nth atom

$$-m \cdot \frac{\partial^2 u_n(x,t)}{\partial t^2} + \frac{\partial F}{\partial x} dx = 0 \Longrightarrow m \cdot \frac{\partial^2 u_n(x,t)}{\partial t^2} = \sum_{j \neq n} \left[-\frac{\partial^2 V}{\partial x^2}\bigg|_{x_n - x_j} (u_n(x,t) - u_j(x,t)) \right] \tag{2.51}$$

Where $u_j(x,t)$ is the displacement from the equilibrium of the n-th atom. A solution of the sort $u_n(x,t) = Ae^{i\left(\omega t - k x_n^{eq}\right)} = Ae^{i(\omega t - kna)}$ will be a valid one as a consequence of the periodicity and translational symmetry. Then the frequency, $\omega(k)$, of the excitation a harmonic crystal is

$$
\begin{aligned}
-m\cdot\omega^2\cdot Ae^{i\left(\omega t-kx_n^{eq}\right)} &= \sum_{j\neq n}\left[-\frac{\partial^2 V}{\partial x^2}\bigg|_{x_n-x_j} A\left(e^{i(\omega t-kx_n)}-e^{i(\omega t-kx_j)}\right)\right]\Longrightarrow \\
\omega^2(k) &= \frac{1}{m}\sum_{j\neq n}\left[-\frac{\partial^2 V}{\partial x^2}\bigg|_{x_n-x_j}\left(1-e^{ik(x_n-x_j)}\right)\right] = \frac{1}{m}\sum_{j\neq n}\left[-\frac{\partial^2 V}{\partial x^2}\bigg|_{x_n-x_j}\left[1-\cos\left(k\left(x_n-x_j\right)\right)\right]\right] \\
\omega^2(k) &= \frac{2}{m}\sum_{j\neq n}\left[-\frac{\partial^2 V}{\partial x^2}\bigg|_{x_n-x_j}\sin^2\left(\frac{k\left(x_n-x_j\right)}{2}\right)\right] \\
\omega^2(k) &= \frac{2}{m}\sum_{n=1}^{\infty}\left[-\frac{\partial^2 V}{\partial x^2}\bigg|_{x=an}\sin^2\left(\frac{kan}{2}\right)\right] \quad \text{where} \quad a=\rho^{-1}
\end{aligned}
\tag{2.52}
$$

So, finally, in order to obtain the excitation spectrum we need to carry out the summation over images of the Hessian matrix

$$
\omega(k) = \sqrt{\frac{2}{m}\sum_{n=1}^{\infty}\left[-\frac{\partial^2 V}{\partial x^2}\bigg|_{\frac{n}{\rho}}\sin^2\left(\frac{kn}{2\rho}\right)\right]} \tag{2.53}
$$

The correction to the energy per particle correction can be obtained by the summation of the energy of the zero-point motion of the atoms. It is

$$
\begin{aligned}
\frac{\Delta E}{N} &= \int_{BZ}\frac{1}{\ell_{BZ}}\frac{\hbar\omega(k)}{2}dk = \frac{1}{2\pi\rho}\int_{-\pi\rho}^{\pi\rho}\frac{\hbar\omega(k)}{2}dk = \frac{\hbar}{2\pi\rho}\int_0^{\pi\rho}\omega(k)dk = \\
&= \frac{\hbar}{2\pi\rho}\int_0^{\pi\rho}\sqrt{\frac{2}{m}\sum_{n=1}^{\infty}\left[-\frac{\partial^2 V}{\partial x^2}\bigg|_{\frac{n}{\rho}}\sin^2\left(\frac{kn}{2\rho}\right)\right]}dk = \frac{\sqrt{\hbar^2/m}}{\sqrt{2}\pi\rho}\int_0^{\pi\rho}\sqrt{\sum_{n=1}^{\infty}\left[-\frac{\partial^2 V}{\partial x^2}\bigg|_{\frac{n}{\rho}}\sin^2\left(\frac{kn}{2\rho}\right)\right]}dk
\end{aligned}
\tag{2.54}
$$

where BZ is the first Brillouin zone and so the total energy of the harmonic crystal will be

$$
\frac{E_{HC}}{N} = \left(\sum_{i=1}^{\infty}V\left(\frac{i}{\rho}\right)\right) + \frac{\sqrt{\hbar^2/m}}{\sqrt{2}\pi\rho}\int_0^{\pi\rho}\sqrt{\sum_{n=1}^{\infty}\left[-\frac{\partial^2 V}{\partial x^2}\bigg|_{\frac{n}{\rho}}\sin^2\left(\frac{kn}{2\rho}\right)\right]}dk \tag{2.55}
$$

3. *Methods and tools*

In order to find the properties of complex quantum systems we will resort to quantum Monte Carlo methods that will be described in this Chapter. It is also necessary to have the definitions of the main quantities relevant in the description of the system either for their connection to different theories or for being observables which can be measured in experiments.

3.1 Quantum Monte Carlo methods

In order to obtain an accurate description of the properties of many-body quantum systems, described by the Schrödinger equation, there exist a group of stochastic methods under the name of Quantum Monte Carlo, that apply the Monte Carlo method for carrying out a multidimensional integration needed in the different schemes of QMC.

Here we will focus on two of versions of MC techniques designed for the study of the ground state properties of the systems, i.e. at $T = 0K$. Namely, we will consider variational (VMC) and diffusion (DMC) Monte Carlo methods. For more information of DMC and VMC methods, see references [23] and [26]

3.1.1 Metropolis algorithm

Typically, numerical routines used to produce random numbers generate flat distributions. Instead, in a variational calculation, we need to sample the square root of the trial w.f. This can be done by using metropolis algorithm.

The sampling from a random probability distribution is needed for both DMC and VMC methods,and so a brief description is presented here. In this section x denotes a point in a N-dimensional phase space, $x = \{x_1, \ldots, x_N\}$.

The Metropolis-Hasting algorithm provides a set of instructions for sampling from a given probability distribution using a Markov process provided the existence and uniqueness of an stationary distribution. The algorithm consists in the following:

1. Start with an initial state (x) for the probability distribution.

2. Propose a new state (x') obtained from $x + \delta x$ with δx a displacement obtained from a symmetric probability density function.

3. The new state will be accepted with probability 1 if $\frac{P(x')}{P(x)} > 1$ and with probability $\frac{P(x')}{P(x)}$ if $\frac{P(x')}{P(x)} < 1$

4. Turn to 2.

So, after sufficient number of steps of the Metropolis algorithm, the technique will be sampling accordingly to the desired probability distribution.

3.1.2 Variational Monte Carlo Method

In the following we are going to describe the Variational Monte Carlo technique. VMC is a simple technique employed for solving multidimensional integrals from stochastic integration, and which paired with some optimization methods approximates the ground-state energy by means refining a trial wave function dependent on a set of parameters, $\Psi(x, a_i)$.

In VMC, the energy of a state $|\Psi\rangle$ is computed as the expectation value of the Hamiltonian over the state $|\Psi\rangle$

$$\langle E\rangle = \frac{\langle \Psi \mid H \mid \Psi\rangle}{\langle \Psi \mid \Psi\rangle} = \frac{\int dx \Psi^*(x) H \Psi(x)}{\int dx \Psi^*(x)\Psi(x)} \geq E_0 \tag{3.1}$$

where the $\langle \Psi \mid \Psi\rangle$ has only the objective of taking into account properly the normalization of the wave function, and E_0 is the ground state energy. Then, integral (3.1) can be understood (in the spirit of Monte Carlo method) as the average of some magnitude over sequence x_i (trajectory of a walker) in the phase space.

$$\langle E\rangle = \frac{\int dx \left|\Psi\right|^2 \left(\frac{H\Psi(x)}{\Psi(x)}\right)}{\int dx \left|\Psi\right|^2} = \lim_{n\to\infty} \frac{1}{n} \sum_{i=1}^{n} \left(\frac{H\Psi|_{x_i}}{\Psi|_{x_i}} \right) \tag{3.2}$$

Walkers positions x_i are distributed according to a probability distribution function generated by the trial wave function.

$$P(x) = \frac{\left|\Psi(x)\right|^2}{\int dx \left|\Psi(x)\right|^2} \tag{3.3}$$

It can be interesting to notice that there are two different ways of estimating the Kinetic energy. The integral for the kinetic energy can be rewritten by integrating by parts

$$\langle K\rangle = -\int_{-\infty}^{\infty} \Psi^* \vec{\nabla}^2 \Psi dx = -\int_{-\infty}^{\infty} \left|\Psi\right|^2 \left(\frac{\vec{\nabla}^2 \Psi}{\Psi} \right) dx \tag{3.4}$$

$$\langle K\rangle = -\left. \Psi \vec{\nabla} \Psi \right|_{-\infty}^{+\infty} + \int_{-\infty}^{\infty} \vec{\nabla}\Psi \cdot \vec{\nabla}\Psi dx = +\int_{-\infty}^{\infty} \left|\Psi\right|^2 \left(\frac{\vec{\nabla}\Psi}{\Psi} \right) \cdot \left(\frac{\vec{\nabla}\Psi}{\Psi} \right) dx \tag{3.5}$$

It will be helpful to notice another identity. We can do from the equations (3.4) and (3.5) the following, that will be used later

$$\int_{-\infty}^{\infty} \Psi \vec{\nabla}^2 \Psi d\vec{R} = \frac{1}{2} \int_{-\infty}^{\infty} \left(\Psi \nabla^2 \Psi - \nabla\Psi \cdot \nabla\Psi \right) d\vec{R} \tag{3.6}$$

Then in summary, the method relies on Monte Carlo technique to compute multidimensional exactly integrals in an efficient way.

The other key to understand the process is the variational principle, which implies that the ground state is the one with the minimum energy. To demonstrate that, we can expand the wave function in terms of eigenfunctions of the Hamiltonian

$$|\Psi\rangle = \sum_n c_n |\Psi_n\rangle \tag{3.7}$$

the mean value of the energy can be computed as

$$\langle E\rangle = \frac{\sum_{n=0}^{\infty} |c_n|^2 \langle \Psi_n \mid H \mid \Psi_n\rangle}{\sum_{n=0}^{\infty} |c_n|^2} = \frac{|c_0|^2 \langle \Psi_0 \mid H \mid \Psi_0\rangle}{\sum_{n=0}^{\infty} |c_n|^2} + \frac{\sum_{n=1}^{\infty} |c_n|^2 \langle \Psi_n \mid H \mid \Psi_n\rangle}{\sum_{n=0}^{\infty} |c_n|^2} = \langle E_0\rangle + \Delta^2 \tag{3.8}$$

providede Ψ is not orthogonal to Ψ_0. Therefore the energy computed with the VMC technique provides a rigorous upper bound for the fundamental or ground-state energy as the trial wave function approaches to the wave function of the fundamental state.

Then the problem of finding the ground state energy of the system ends up being an optimization problem, whenever it was possible to properly parametrize the wave function

$$a \in \mathcal{A} \subseteq \mathbb{R}^n \qquad \text{find} \qquad a_0 \in \mathcal{A} \quad s.t. \quad \langle E\rangle (a_0) \leq \langle E\rangle (a) \qquad \forall a \in \mathcal{A} \tag{3.9}$$

also, in addition to minimize the energy, the ground state minimizes fluctuations.

3.1.3 Diffusion Monte Carlo Method

In this section the diffusion Monte Carlo method is introduced. The imaginary time-dependent Schrödinger equation can be written as

$$-\frac{\partial \Psi(R,t)}{\partial t} = (H - E)\Psi(R,t) \tag{3.10}$$

with a formal solution of the form $\Psi(t) = \exp\left[-t\,(H-E)\right]\Psi(0)$ or expressed in terms of the eigen functions of the Hamiltonian

$$\Psi(R,t) = \sum_n c_n \phi_n(R,0) \exp\left[t\,(E - E_n)\right] \tag{3.11}$$

or in coordinate representation

$$\langle R' \mid \Psi(t)\rangle = \int \underbrace{\langle R' \mid \exp\left[-(H-E)t\right] \mid R\rangle}_{G(R',R,t)} \langle R' \mid \Psi(0)\rangle \, dR \tag{3.12}$$

where $G(R', R, t)$ is the Green's function. This equation, for $H = -D\Delta + V(R)$, can be understood as a diffusion equation

$$-\frac{\partial \Psi(R,t)}{\partial t} = \underbrace{-D\Delta\Psi(R,t)}_{diffusion} + \underbrace{\left[V(R) - E\right]\Psi(R,t)}_{creation/annihilation} \tag{3.13}$$

where $D = \frac{\hbar^2}{2m}$ is the diffusion constant. The statistical accuracy can be improved introducing a guiding function $\Psi_T(R)$ in the sense of importance sampling. Then $f(R,t) = \Psi_T(R)\Psi(R,t)$.

$$-\frac{\partial f(R,t)}{\partial t} = -D\Delta f(R,t) + D\vec{\nabla}\cdot\left[\vec{F}f(R,t)\right] + (E_L(R) - E)\, f(R,t) \tag{3.14}$$

where

$$\vec{F} = \frac{2}{\Psi_T(R)}\vec{\nabla}\Psi_T(R) \qquad \textit{Drift Force} \tag{3.15}$$

and

$$E_L(R) = \frac{1}{\Psi_T(R)}H\Psi_T(R) \qquad \textit{Local Energy} \tag{3.16}$$

The solution of this new equation can be written as we mentioned above and solved recursively in time

$$\langle R' \,|\, \Psi(t+\delta t)\rangle = \int G\left(R', R, \delta t\right) \langle R' \,|\, \Psi(t)\rangle \, dR \tag{3.17}$$

where

$$G\left(R', R, \delta t\right) = \left\langle R' \,\middle|\, \exp\left[\left(-D\Delta + D\left(\vec{\nabla}\cdot\vec{F} + \vec{F}\cdot\vec{\nabla}\right) + E_L(R) - E\right)\delta t\right] \,\middle|\, R\right\rangle = \langle R' \,|\, \exp\left[-A\delta t\right] \,|\, R\rangle \tag{3.18}$$

The calculation of Green's function in a many body system, generally, is not possible analytically, so an approximation can be done to the total Green's function. If we call A the operator in the exponential of the Green's function, we can divide it in its parts, so

$$A_1 = -D\Delta \qquad A_2 = D\left(\vec{\nabla}\cdot\vec{F} + \vec{F}\cdot\vec{\nabla}\right) \qquad A_3 = E_L(R) - E \tag{3.19}$$

each one fulfilling

$$G_i = \langle R' \,|\, \exp\left[-A_i\delta t\right] \,|\, R\rangle \qquad -\partial_t G_i = A_i G_i \tag{3.20}$$

Then the Green function of the whole system can be expanded for small times

$$A = \exp(-A\cdot\delta t) = e^{-\frac{1}{2}A_3\delta t}e^{-\frac{1}{2}A_2\delta t}e^{-\frac{1}{2}A_3\delta t}e^{-A_1\delta t}e^{-\frac{1}{2}A_2\delta t}e^{-\frac{1}{2}A_3\delta t} \tag{3.21}$$

The approximate Green function is

$$\begin{aligned} G(R', R, t) = (4\pi Dt)^{-3N/2} \exp\left[\frac{E - E_L(R) - E_L(R')}{2}\cdot t\right] \\ \cdot \exp\left[-\frac{\left(R' - R - \frac{1}{2}Dt(F(R) + F(R'))\right)^2}{4Dt}\right] + O(t^3) \end{aligned} \tag{3.22}$$

or in less accurate $O(t^2)$ but more simple form

$$G(R', R, t) = (4\pi Dt)^{-3N/2} \exp\left[\frac{E - E_L(R) - E_L(R')}{2}\cdot t\right] \cdot \exp\left[-\frac{\left(R' - R - Dt\cdot F(R)\right)^2}{4Dt}\right] \tag{3.23}$$

Practical implementation

Algorithmically, the key to solve the problem using the DMC method is to interpret $G(R, R', t)$ as a non-normalized transition probability of changing from a set of points (walkers) defining $\Psi(R)$ to another set of points defining $\Psi(R')$. Then the steps to proceed in order to solve the problem are

1. Choose a guiding wave function that must be accurate enough in order to capture correctly the physics of the described phase.

2. Generate a set of initial walkers following a distribution given by a trial wave function Ψ_T.

3. Make this set of initial walkers, the initial distribution, evolve according the Green's function. The evolution can be split in three main parts, one that has to deal with the diffusive part, the one related to the drift force and the one about branching, which changes the normalization of the Green's function. So first of all from one of the initial walkers

$$R_{(1)} = R_{(0)} + DtF(R)$$

then

$$R_{(2)} = R_{(1)} + \delta$$

where the displacement δ comes from a d·N-variate Gaussian distribution, 'd' being the dimensionality of the space.

$$p(\delta) = \frac{1}{(4\pi Dt)^{dN/2}} \exp\left(-\frac{\delta^2}{4Dt}\right)$$

And the last step is to compute the multiplicity of the walkers (branching) depending on the energy, giving more weight to walkers with lower energy. We can compute the number of descendants of a walker as

$$M = Int\left[\exp\left\{\left(E - E_L(R) - E_L(R')\right)t\right\} + \gamma\right]$$

where γ is a random number distributed uniformly between 0 and 1. The new walker is replicated M times (or killed when M=0) and added to the list of walkers. If we repeat this set of steps for every walker the population will not always tend to a steady value, and so is better to control the population externally applying an artificial control.

To be precise, we introduce a factor of the form

$$M' = \begin{cases} floor\left[\dfrac{M}{M_{max}} \cdot \dfrac{M_{max} + M_{min}}{2} + U(0,1)\right] & if\ M > M_{max} \\ floor\left[\dfrac{M}{M_{min}} \cdot \dfrac{M_{max} + M_{min}}{2} + U(0,1)\right] & if\ M < M_{min} \end{cases} \tag{3.24}$$

that corrects the multiplicity if needed, preventing from moving away from the desired number of walkers that mantain the simulation stable.

3.2 Error estimation

The analysis of the error in the Monte Carlo methods is one of the key aspects to take into account when interpreting the data obtained from the simulations. The following plot reflects the typical data of the energy measurements inside a VMC/DMC program.

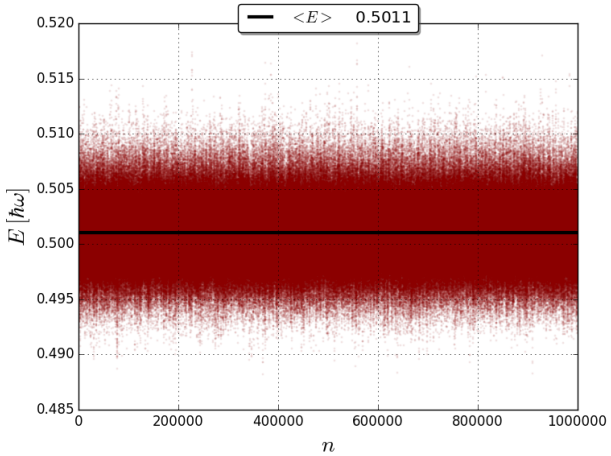

Figure 3.1: A typical dependence of a local energy of an harmonic oscillator on the simulation time is shown

The bias in the estimation of the energy has different aspects or causes, like the number of particles in the simulation box, the time step and the number of walkers (in DMC). The statistical error due to the use of a finite number of samples or measurement.

3.2.1 Statistical Error

In order to determine the statistical error we can proceed in a number of ways. Here we will consider the block average technique. If we define the average value $\langle x \rangle$ and variance σ as

$$\langle x \rangle = \frac{1}{N}\sum_{i}^{N} x_i \qquad \langle x^2 \rangle = \frac{1}{N}\sum_{i}^{N} x_i^2 \qquad \sigma = \sqrt{\frac{\langle x^2 \rangle - \langle x \rangle^2}{N-1}} \tag{3.25}$$

where N is the number of samples, and x_i the value of a given sample, the value of σ can be considered as the error of the mean value obtained from the data, given the samples are

not correlated. Since the samples in a Metropolis random walk are indeed correlated, we can proceed to estimate the error by dividing the data in blocks and averaging over this different blocks considering the new set of averages as new set of samples and proceeding in the same way to compute σ. If we try this block averaging for different sizes of the blocks, we will find that the error computed in this new different way tends to a maximum value increasing the number of samples per block. This value is a good estimation of the error of the mean of the data set.

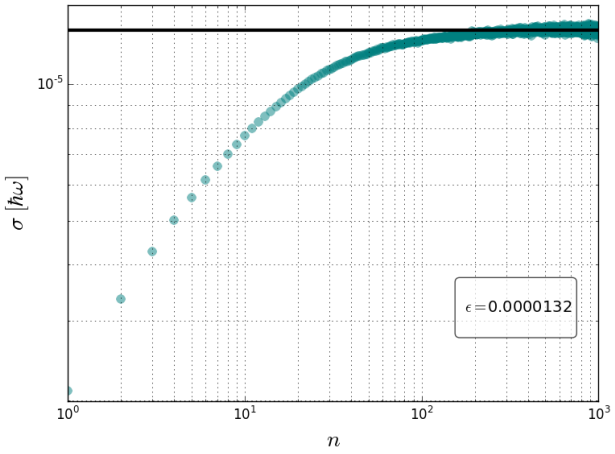

Figure 3.2: Variance in terms of the number of samples per bin

Here horizontal axis show the number samples per bin, and we can see that for small number of samples per box the error goes to a minimum value, while for large number the error is maximum and constant, since the variance $\sqrt{\langle x^2\rangle - \langle x\rangle^2}$ grows with $\sqrt{N}$.

Apart from the statistical error, there exist other kinds of error in the numerical simulations. On one hand we have to correct the effect introduced by the finite size of the simulation box and the boundary conditions, on the other hand we have to deal with the error associated with the choice of an accurate guiding wave function, that is ensure that the number of walkers is large enough.

3.2.2 Finite size effects

The finiteness of the simulation box, or the number of particles, is one of the causes of systematic error, that arises from the lack of long range correlations, both kinetic and potential. This can be corrected by adding the so called 'tail corrections' that mainly consist in integrate the potential and kinetic contribution for large distances assuming that the radial distribution function $g(r)$ remains constant and equals to one, for large enough distances. This calculations will be discussed and performed for our particular system in Section 4.3.1

3.2.3 Walkers and time step

The DMC method we also have to take into account the effect of the finite number of walkers involved in the branching problem and so in a fundamental aspect of the method. Also the time-step that has to deal with drift, diffusion and branching and that has to be tuned in order to find the correct energy while keeping the error (statistical) low enough. It is common to estimate the optimal DMC time step as the 10% of the time step in VMC, with all particles moved simultaneously.

However it is suitable to make an study of the different magnitudes computed (energy, radial distribution function, static structure factor, etc) in terms of these parameters in order to have a correct idea of the error in their values.

3.3 System properties and Pure estimator

In this Section the main quantities of interest and concepts related to them are exposed. We will review the concepts of one-body density matrix, pair correlation function, static structure factor, energy and discuss their implementation in MC code.

3.3.1 One-body density matrix

The normalized one-body density matrix is related to the probability of finding a particle at a position $x_i + x$ once removed from position x_i.

$$\rho\left(x\right) = \int \psi^{*}\left(x_1, x_2, \ldots, x_N\right) \psi\left(x_1 + x, x_2, \ldots, x_N\right) dx_2 \ldots dx_N \tag{3.26}$$

In terms of MC approach it can be computed from

$$\begin{aligned} \rho\left(x\right) &= \int \psi^{*}\left(x_1, x_2, \ldots, x_N\right) \psi\left(x_1 + x, x_2, \ldots, x_N\right) dx_2 \ldots dx_N = \\ &= \int \left|\psi\left(x_1 + x, x_2, \ldots, x_N\right)\right|^2 \frac{\psi\left(x_1 + x, x_2, \ldots, x_N\right)}{\psi\left(x_1, x_2, \ldots, x_N\right)} dx_1 \ldots dx_N = \\ &= \left\langle \frac{\psi\left(x_1 + x, x_2, \ldots, x_N\right)}{\psi\left(x_1, x_2, \ldots, x_N\right)} \right\rangle_{|\psi|^2} \end{aligned} \tag{3.27}$$

that in the case of the variational method is to evaluate this integral from the variational wave function. In order to improve statistics we can average over all the particles in the system, so

$$\rho(x) = \frac{1}{N} \left\langle \sum_{i=1}^{N} \frac{\psi_T\left(x_1, \ldots, x_i + x, \ldots, x_N\right)}{\psi_T\left(x_1, \ldots, x_N\right)} \right\rangle_{|\psi_T|^2} \tag{3.28}$$

3.3.2 Pair correlation function

The pair correlation function or radial distribution function describes how the density of particles varies arround a generic particle in the system. Mathematically it can be expressed, for an homogeneous system, as

$$g(r) = \frac{1}{dV}\frac{1}{N\rho}\sum_{i=1}^{N}\sum_{k\neq i}^{N}\delta\left(r - |r_k - r_i|\right) \tag{3.29}$$

that in our case (in a one-dimensional system) and in a practical way it can be computed in the following way

$$g(r) = \frac{n_{bins}}{N^2 \cdot n_{mea}}\sum_{i=1}^{N}\sum_{k>i}^{N} 2 \cdot \delta\left(r - |r_k - r_i|\right) \tag{3.30}$$

where the computation (the histogram where the average is done) is made in a grid of n_{bins} cells. The magnitude n_{mea} is the number of times that the quantity is averaged. N is the number of particles in the simulation box.

The pair correlation function can be normalized by the mean density of the simulation box, so $g(\infty) = 1$. For systems composed by different species, one can define a radial distribution function for each specie, however it is not our case.

3.3.3 Static Structure Factor

The static structure factor represents the scattering intensity of the given system divided by the scattering intensity of a random and uncorrelated distribution of atoms with the same mean density. This quantity is relevant since it can be experimentally measured, it is accessible from a sample of the system. The static structure factor $S(k)$ is defined as

$$S(k) = \frac{1}{N}\left\langle \rho_k \rho_{-k} \right\rangle = \frac{1}{N}\left\langle \sum_{i=1}^{N}\sum_{j=1}^{N} exp\left[-ik\left(r_i - r_j\right)\right] \right\rangle \tag{3.31}$$

Also it is related by the Fourier Transform to the pair correlation function

$$\begin{aligned}
S(k) &= \frac{1}{N}\left\langle \int dr \int dr' exp\left[-ik(r-r')\right]\left(\sum_{i=1}^{N}\delta(r-r_i)\sum_{j=1}^{N}\delta(r'-r_j)\right)\right\rangle = \\
&= 1 + \frac{1}{N}\left\langle \int dr \int dr' exp\left[-ik(r-r')\right]\left(\sum_{i=1}^{N}\delta(r-r_i)\sum_{j\neq i}^{N}\delta(r'-r_j)\right)\right\rangle = \\
&= 1 + \frac{1}{N}\left\langle \int dr \int dr' exp\left[-ik(r-r')\right]\rho(r,r')\right\rangle = \\
&= 1 + \frac{1}{N}\left\langle \int dr \int dr' exp\left[-ik(r-r')\right]\rho^2 g(r,r')\right\rangle = 1 + \rho\int exp\left(-ikr\right) g(r) dr
\end{aligned} \tag{3.32}$$

however this expression for $S(k)$ does not converge due to the behaviour of $g(r)$. Then we can transform this expression substracting $\int exp\,(-ikr)\,dr = 0$

$$S(k) = 1 + \rho \int exp\,(-ikr)\,[g(r) - 1]\,dr \tag{3.33}$$

3.3.4 Pure Estimators. Extrapolation technique.

In order to study the properties of the system from the DMC and VMC methods explained above we can make use of the pure estimator in order to obtain a higer degree of accuracy. From the variational method we obtain the variational average

$$\langle A \rangle_{VMC} = \frac{\langle \Psi_T \,|\, A \,|\, \Psi_T \rangle}{\langle \Psi_T \,|\, \Psi_T \rangle} \tag{3.34}$$

and from the DMC method we have a 'mixed' one

$$\langle A \rangle_{DMC} = \frac{\langle \phi_0 \,|\, A \,|\, \Psi_T \rangle}{\langle \phi_0 \,|\, \Psi_T \rangle} \tag{3.35}$$

However, what we want to obtain the ground-state average of the observable, that is

$$\langle A \rangle_{pure} = \frac{\langle \phi_0 \,|\, A \,|\, \phi_0 \rangle}{\langle \phi_0 \,|\, \phi_0 \rangle} \tag{3.36}$$

The technique of pure estimators is based on carrying out the weighted averages according to

$$\langle A \rangle_{pure} = \frac{\langle \phi_0 \,|\, A \,|\, \phi_0 \rangle}{\langle \phi_0 \,|\, \phi_0 \rangle} = \frac{\left\langle \phi_0 \,\middle|\, A \frac{\phi_0}{\Psi_T} \,\middle|\, \Psi_T \right\rangle}{\left\langle \phi_0 \,\middle|\, \frac{\phi_0}{\Psi_T} \,\middle|\, \Psi_T \right\rangle} \tag{3.37}$$

Alternatively, when the trial wave function is close to the ground-state one, we write the ground state function as $\phi_0 = \Psi_T + \delta\Psi$. We can expand the pure average in the following way

$$\begin{aligned} \langle A \rangle_{pure} &= \langle \psi_0 \,|\, A \,|\, \psi_0 \rangle = \langle \Psi_T + \delta\Psi \,|\, A \,|\, \Psi_T + \delta\Psi \rangle = \\ &= \langle \Psi_T \,|\, A \,|\, \Psi_T \rangle + \langle \Psi_T \,|\, A \,|\, \delta\Psi \rangle + \langle \delta\Psi \,|\, A \,|\, \Psi_T \rangle + \langle \delta\Psi \,|\, A \,|\, \delta\Psi \rangle = \\ &= \langle \Psi_T \,|\, A \,|\, \Psi_T \rangle + 2\,\langle \Psi_T \,|\, A \,|\, \delta\Psi \rangle + \langle \delta\Psi \,|\, A \,|\, \delta\Psi \rangle = \\ &= \langle \Psi_T \,|\, A \,|\, \Psi_T \rangle + 2\,\langle \Phi_0 \,|\, A \,|\, \delta\Psi \rangle - \langle \delta\Psi \,|\, A \,|\, \delta\Psi \rangle \end{aligned} \tag{3.38}$$

and knowing that

$$\begin{aligned}\langle\phi_0 \,|\, A \,|\, \delta\Psi\rangle &= \langle\Psi_T + \delta\Psi \,|\, A \,|\, \phi_0 - \Psi_T\rangle = \langle\Psi_T \,|\, A \,|\, \phi_0\rangle - \langle\Psi_T \,|\, A \,|\, \Psi_T\rangle + \langle\delta\Psi \,|\, A \,|\, \phi_0 - \Psi_T\rangle = \\ &= \langle\Psi_T \,|\, A \,|\, \phi_0\rangle - \langle\Psi_T \,|\, A \,|\, \Psi_T\rangle + \langle\delta\Psi \,|\, A \,|\, \delta\Psi\rangle\end{aligned} \tag{3.39}$$

we end up with the final expression

$$\langle A\rangle_{pure} = 2\,\langle\Psi_T \,|\, A \,|\, \phi_0\rangle - \langle\Psi_T \,|\, A \,|\, \Psi_T\rangle + \langle\delta\Psi \,|\, A \,|\, \delta\Psi\rangle = 2\,\langle A\rangle_{DMC} - \langle A\rangle_{VMC} + O\left(\delta\Psi^2\right) \tag{3.40}$$

There exists a second estimator of the same order of accuracy, which is

$$\langle A\rangle_{pure} = \frac{\left(\langle A\rangle_{DMC}\right)^2}{\langle A\rangle_{VMC}} + O\left(\delta\Psi^2\right) \tag{3.41}$$

The agreement of both estimators is useful to verify the reliability of the extrapolation method. However, some times they coincide but do not reproduce the real “pure” estimator.

4. *One-dimensional Hydrogen*

Our goal is the description and accurate simulation of hydrogen atoms confined to a one dimensional geometry at 0K. A possible realization is a hydrogen 'gas' confined through harmonic confinement that restricts drastically the movement in two of the spatial dimensions. Since there are three stable isotopes of hydrogen (protium, deuterium and tritium) with different characteristics and statistics, we will study all of them by means of Monte Carlo techniques (VMC and DMC) and we will discuss the obtained results.

4.1 The model Hamiltonian

The one dimensional hydrogen gas can be precisely described in terms of the following Hamiltonian

$$\hat{\mathcal{H}} = -\frac{\hbar^2}{2m_H}\sum_n \Delta_n + \sum_{i<j} V\left(|x_i - x_j|\right) \tag{4.1}$$

For the potential interaction we use the JDW form, obatined on Jamieson, Dalgarno, and Wolniewicz (JDW) [14, 15] that was tested and proved to be essentially exact. A comparison between different interaction potentials for H-H has been reported in the work of L. Vranješ Markić, J. Boronat and J. Casulleras. [16]

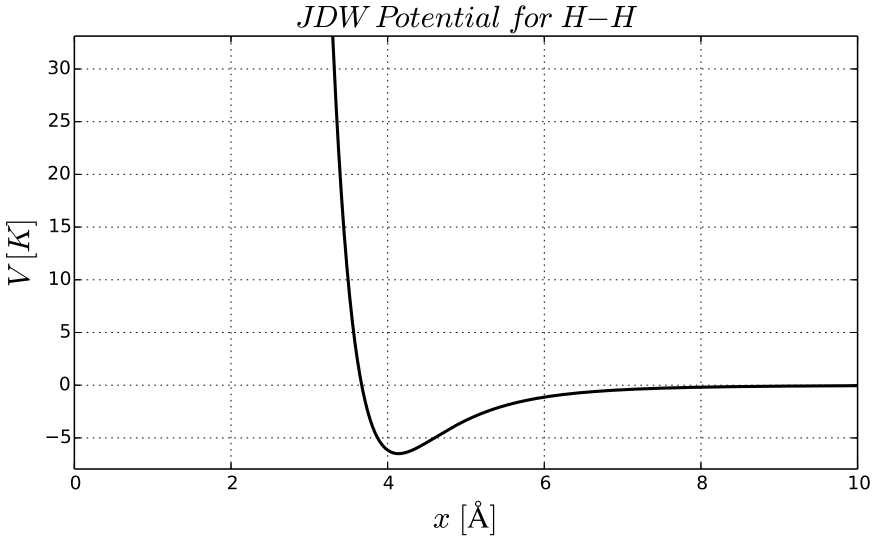

Figure 4.1: Detail of JDW potential for spin polarized hydrogen

The hydrogen-hydrogen interaction potential is shown in figure 4.1. The potential for short distances has a repulsive core, it presents a depth with a minimum of -6.49K at $x = 4.14$Å. For large distances there is an attractive tail and it is expected to be similar to the one from the description of the interaction between induced electric dipoles (we can think in two hydrogen atoms as two dipoles formed by the electron-proton pair, interacting in an induced way), it is a power law with a exponent equal to 6.

Figure 4.2 analyses the shape of the tale in the log-log scale. A power law dependence of the form $V(x) = -\left(\frac{a}{r}\right)^b$ would result in a straight line

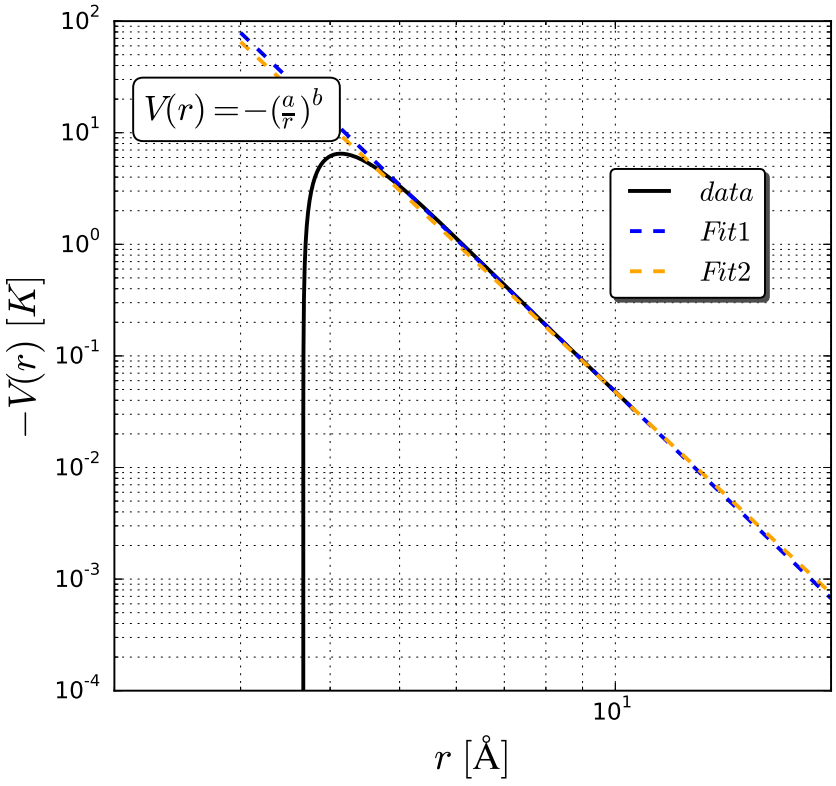

Figure 4.2: Potential fit for large distances

For the best fit, we find $a = 6.11\mathring{A}$ and $b = 6.18$ (the line in blue) for $r > 5\mathring{A}$, however we will use a more physical fit keeping the exponent $b = 6$ (dashed orange line)

$$V(r)\Big|_{r>10.5824\text{Å}} = -\left(\frac{a}{r}\right)^6 \text{K} \quad \text{where} \quad a \sim 6.0056\text{Å} \tag{4.2}$$

The short distances behaviour, dominant at large densities is reported in figure 4.3, in which we have fitted an exponential law that appears to be suitable at very short distances.

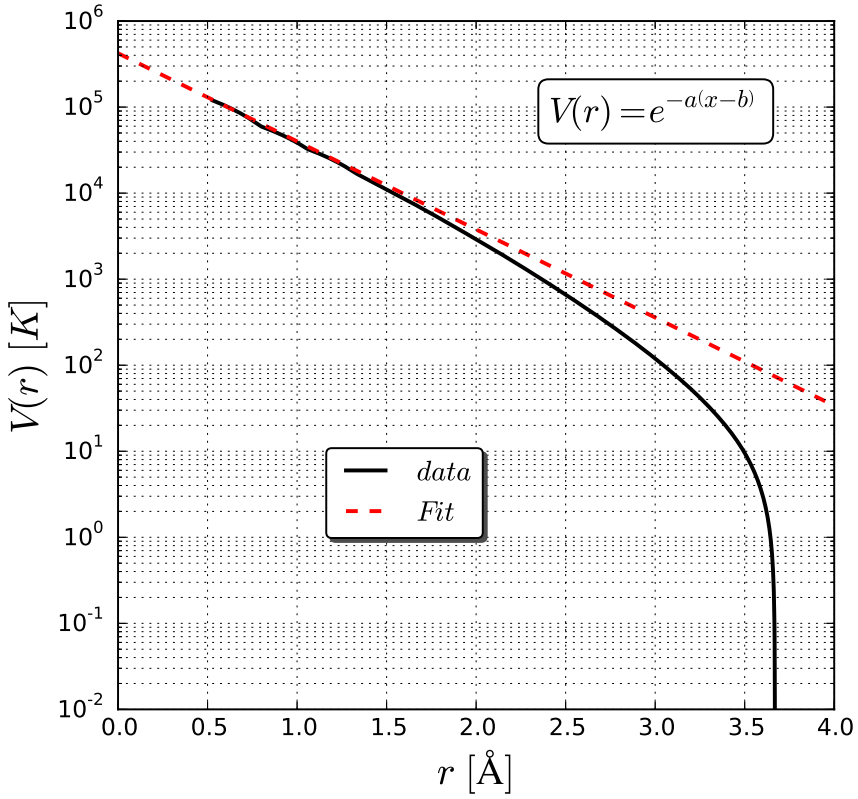

Figure 4.3: Potential wall shape

The best fit provides $a \sim 2.36\mathring{A}^{-1}$ and $b \sim 5.50\mathring{A}$. This fit works well for distances $r \lesssim 1.5\mathring{A}$.

In any case, the smallest distance for which the interaction potential was defined in [14, 15] is $r = 0.5\mathring{A}$.

4.2 Dimensionless Schrödinger Equation

It is convenient to rewrite Schrödinger equation

$$-\frac{\hbar^2}{2m_H}\sum_n \frac{\partial^2\Psi(x)}{\partial x^2} + \sum_{i<j} V\left(|x_i - x_j|\right) = \epsilon\Psi(x) \tag{4.3}$$

by introducing dimensionless units $\tilde{\epsilon} = \epsilon/\epsilon_o$, $\tilde{x} = x/x_o$and $\tilde{V} = V/\epsilon_o$.

All distances will be expressed in Å, (that is $x_o = 1\mathring{A}$). When performing simulations, we will use $\epsilon_o = \frac{\hbar^2}{mx_o^2}$ as a unit of energy, converting later the energies to Kelvins.

$$-\frac{1}{2}\sum_n \frac{\partial^2\Psi(\tilde{x})}{\partial\tilde{x}^2} + \left(\sum_{i<j}\tilde{V}\left(|\tilde{x}_i - \tilde{x}_j|\right) - \tilde{\epsilon}\Psi(\tilde{x})\right) = 0 \tag{4.4}$$

The characteristic energy scale is relevant to the kinetic-energy term in (4.3) and depends on the mass of the different isotopes, which will be the main differentiator parameter.

$$\frac{\hbar^2}{m_H}\frac{1}{x_o^2\epsilon_o} = 1 \longrightarrow \epsilon_o = \frac{\hbar^2}{m x_o^2} \tag{4.5}$$

Table 4.2 reports the isotope mass as well as the conversion factor.

Isotope	*mass* (u)	ϵ_o (J)	ϵ_o (K)
Hydrogen H	1.00794	$6.64459 \cdot 10^{-22}$	48.127
Deuterium ^2H	2.01410	$3.326137 \cdot 10^{-22}$	24.0911
Tritium ^3H	3.01605	$2.220571 \cdot 10^{-22}$	16.08365

where the energy expressed in Kelvins is $\epsilon(K) = \epsilon(J)/k_B$, being k_B the Boltzmann constant.

This dimensionless version is needed in order to implement the problem numerically since work with too low or too high numbers would result in inaccurate numerical results or even can make calculations impracticable.

4.3 Trial Wave Function and Energy

This trial wave function for the variational Monte Carlo is chosen in the form of a pair Jastrow product. For fermionic isotopes we write the trial wave function in the following way

$$\Psi_{^1H,^3H}(x_1, \ldots, x_N) = \prod_{i<j}^{N} f_2(x_i - x_j) sign\,(x_i - x_j) \tag{4.6}$$

where the function $f_2(x_{ij})$ is constructed by matching the two body scattering solution at short distances and the phononic assymptotics at large distances:

$$f_2(x) = \begin{cases} f_{tbs} & x < R_{par} \\ \left|\sin\left(\dfrac{\pi x}{L}\right)\right|^{1/K_{par}} & x > R_{par} \end{cases} \tag{4.7}$$

Trial wave function depends on two variational parameters R_{par} and K_{par} which we fix by minimizing the variational energy.

The guiding wave function will be slightly different for Hydrogen and Tritium (that are bosons) than for Deuterium (that is a fermion) by virtue of the spin–statistics theorem. From Girardeau's mapping [25] we have that the bosonic wave function will be

$$\Psi_{^2H}(x_1, \ldots, x_N) = \prod_{i<j}^{N} f_2(x_i - x_j) \tag{4.8}$$

As was said in the description of the variational method, we will need to compute the action of the Hamiltonian over the wave function

$$\mathcal{H}\Psi \Longrightarrow \left(-\frac{1}{2}\sum_n \tilde{\Delta}_n + \left(\sum_{i<j} \tilde{V}\left(|\tilde{x}_i - \tilde{x}_j|\right)\right)\right)\Psi(\tilde{x}) \tag{4.9}$$

therefore it will be necessary to compute the Laplacian of the wave function, which can be expressed in terms of the first and second derivatives of the Jastrow f_2 function. First of all we know that

$$\Delta_n \Psi = \nabla_n \cdot \nabla_n \Psi \tag{4.10}$$

so lets compute $\nabla\Psi$

$$\begin{aligned}\nabla_k \Psi = \nabla_k \prod_{i<j}^{N} f(x_{ij}) = \frac{\prod_{i<j}^{N} f(x_{ij})}{\prod_{i\neq k}^{N} f(x_{ik})} \nabla_k \prod_{i\neq k}^{N} f(x_{ik}) = \frac{\prod_{i<j}^{N} f(x_{ij})}{\prod_{i\neq k}^{N} f(x_{ik})} \left(\sum_{i\neq k}^{N} \frac{\nabla_k f(x_{ik})}{f(x_{ik})} \right) \prod_{i\neq k}^{N} f(x_{ik}) \\ = \Psi \sum_{i\neq k}^{N} \frac{\nabla_k f(x_{ik})}{f(x_{ik})}\end{aligned} \tag{4.11}$$

Now we compute the Laplaciand as the divergence of the gradient

$$\nabla_k \cdot \nabla_k \Psi = \nabla_k \left(\Psi \sum_{i\neq k}^{N} \frac{\nabla_k f(x_{ik})}{f(x_{ik})} \right). \tag{4.12}$$

Using that $\nabla \cdot (\psi \mathbf{A}) = \mathbf{A} \cdot \nabla\psi + \psi \nabla \cdot \mathbf{A}$ we can write

$$\Delta_k = \left(\sum_{i\neq k}^{N} \frac{\nabla_k f(x_{ik})}{f(x_{ik})} \right) \cdot \nabla_k \Psi + \Psi \left(\sum_{i\neq k}^{N} \nabla_k \cdot \left(\frac{\nabla_k f(x_{ik})}{f(x_{ik})} \right) \right) \tag{4.13}$$

and from the identity $\nabla \cdot \left(\frac{\mathbf{A}}{g} \right) = \frac{(\nabla \cdot \mathbf{A}) g - \mathbf{A} \cdot \nabla g}{g^2}$ the Laplacian can be written finally as

$$\Delta_k \Psi = \left[\left(\sum_{i\neq k}^{N} \frac{\nabla_k f(x_{ik})}{f(x_{ik})} \right)^2 + \sum_{i\neq k}^{N} \frac{\left[\Delta_k f(x_{ik})\right] f(x_{ik}) - \left[\nabla_k f(x_{ik})\right]^2}{\left(f(x_{ik})\right)^2} \right] \Psi \tag{4.14}$$

that for one dimension is

$$\Delta_k \Psi = \frac{\partial^2 \Psi}{\partial x_k} = \left[\left(\sum_{i\neq k}^{N} \frac{f_k(x_{ik})}{f(x_{ik})} \right)^2 + \sum_{i\neq k}^{N} \frac{\left[f_{kk}(x_{ik})\right] f(x_{ik}) - \left[f_k(x_{ik})\right]^2}{\left(f(x_{ik})\right)^2} \right] \Psi. \tag{4.15}$$

Then, the local kinetic energy will be

$$\mathcal{K}_{loc} = -\frac{1}{2} \sum_{k=1}^{N} \left(\left(\sum_{i\neq k}^{N} \frac{f_k(x_{ik})}{f(x_{ik})} \right)^2 + \sum_{i\neq k}^{N} \frac{\left[f_{kk}(x_{ik})\right] f(x_{ik}) - \left[f_k(x_{ik})\right]^2}{\left(f(x_{ik})\right)^2} \right) \tag{4.16}$$

However we can find a simple formula for the energy, from the so-called Jackson–Feenberg identity (3.6), it is

$$\mathcal{K}_{loc} = -\frac{1}{4} \sum_{k=1}^{N} \left(\sum_{i\neq k}^{N} \frac{\left[f_{kk}(x_{ik})\right] f(x_{ik}) - \left[f_k(x_{ik})\right]^2}{\left(f(x_{ik})\right)^2} \right) = \frac{1}{2} \sum_{i<k}^{N} \left(\frac{f'}{f} \right)^2 - \frac{f''}{f} \tag{4.17}$$

and consequently, the total local energy

$$\mathcal{E}_{loc} = \sum_{i<j}^{N} \frac{1}{2} \left(\left(\frac{f'_{ij}}{f_{ij}} \right)^2 - \frac{f''_{ij}}{f_{ij}} \right) + U_{ij} \tag{4.18}$$

Finally, the general formula for a D-dimensional space is

$$\mathcal{E}_{loc} = \sum_{i<j}^{N} \frac{1}{2} \left(\left(\frac{f'_{ij}}{f_{ij}} \right)^2 - \frac{f''_{ij}}{f_{ij}} - \frac{(D-1)\, f'_{ij}}{r_{ij} f_{ij}} \right) + U_{ij} \tag{4.19}$$

.

4.3.1 Tail correction

In order to estimate the thermodynamic energy from a simulation in a box with periodic boundary conditions, limited in space and particles and with boundary conditions, we must introduce the corrections related to the potential and kinetic energy for long distances. The kinetic energy tail is zero since we compute it from a function where we have imposed tha $f'(L/2) = 0$. However the long-range contribution of the potential energy has to be taken into account. We assume that $g(r = L/2) = 1$ and obtain

$$\frac{\Delta \langle E \rangle}{N} = \frac{\rho}{2} \int_{L/2}^{\infty} g(r) U(r) dr = \frac{\rho}{2} \int_{L/2}^{\infty} U(r) dr \tag{4.20}$$

When the number of particles in our simulation box is large enough, we can approximate the interaction potential by its long-range expansion $V(r) = -\left(\frac{a}{r}\right)^6$. This assumption is expected to work for $\rho < 0.2 \mathring{A}^{-1}$ and leads to

$$\frac{1}{N} \Delta \langle E \rangle = \frac{\rho}{2} \int_{L/2}^{\infty} \left(\frac{a}{r} \right)^6 dr = \frac{a^6 \rho}{2 \cdot 5} \left(\frac{2}{L} \right)^5 = \left(\frac{2^4 a^6}{5} \right) \frac{\rho^6}{N^5} \sim 1.5 \cdot 10^5 \frac{\rho^6}{N^5} \tag{4.21}$$

Here we see that in the low-density regime the correction due to the potential energy is extremely weak and scales as N^{-5}

4.3.2 Quantum statistics

We have mentioned above that the trail wave function will be of the form of a Jastrow wave function

$$\Psi(x_1, \ldots, x_N) = \prod_{i<j}^{N} f_p(x_i - x_j) \qquad \begin{cases} f_p(x) = f_2(x) \text{ (for bosons)} \\ f_p(x) = f_2(x) \cdot sign(x) \text{ (for fermions)} \end{cases} \tag{4.22}$$

however, we have to recall that the term $sign(x_i - x_j)$ is only for taking into account the antysimmetric wave function of fermions, while it is not used in the bosonic wave function.

We will deal with both statistics (fermions and bosons), so the wave function for Hydrogen and Tritium will be symmetric while Deuterium's wave function will be antisymmetric. figure 4.3.2 we show two characteristic examples of the f_p function.

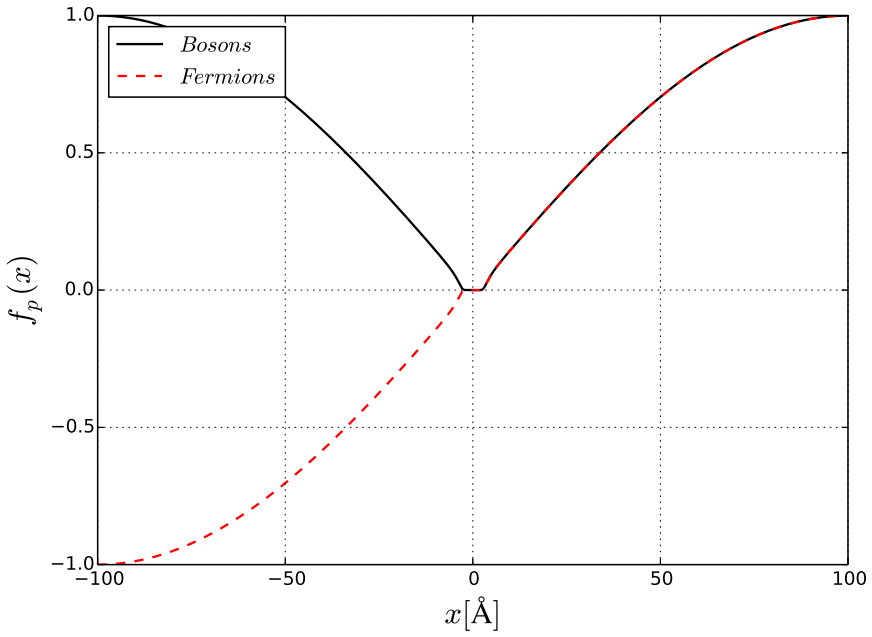

Figure 4.4: Two-body scattering problem comparison for fermions and bosons.

In spite of the different symmetry of the wave function, we can observe that the energetic behaviour of our system is not going to be altered by the statistics of the particle, as we can see in the equation for $\Delta_k \Psi$. The only term that can be changed is the $f_p^{''}(x) f_p(x)$, however it does not depend on the statistics.

$$\frac{d^2 f(x) sign(x)}{dx^2} \cdot f(x) sign(x) = \Big[sign(x) f^{''}(x) \Big] f(x) sign(x) = f^{''}(x) f(x) \tag{4.23}$$

and so the only effective difference between the different isotopes will be its mass in what refers to the metropolis or DMC implementation. However, the parity of the wave function will affect non-local quantities like the one-body density matrix and the momentum distribution.

From figure 4.3.2 we can also see that the two-body scattering solution is a physical one in the sense that we have a zero probability of having two atoms at the same place. In fact, we observe a hard core behaviour since the wave functions vanishes in a region around zero.

4.3.3 Luttinger parameter K

One of the variational parameters of the guiding wave function defines the long-range decay of the Jastrow factor and is related to the Luttinger liquid theory for bosons. The parameter K is defined in the Luttinger liquid theory as an universal parameter [27, 13]

$$K = \frac{v_F}{c} \tag{4.24}$$

where $v_F = \frac{\hbar}{m} k_F$ is the Fermi velocity and c is the speed of sound in the system. The speed of sound can be computed in different ways. On one hand it can be obtained from the compressibility.

$$mc^2 = \frac{\partial P}{\partial \rho} \tag{4.25}$$

This provides a way to obtain the speed of sound from the equation of state $E(\rho)$

$$\begin{aligned} c(\rho) &= \sqrt{\frac{1}{m}\frac{\partial}{\partial \rho}\left(-\frac{\partial E}{\partial \rho}\frac{\partial \rho}{\partial L}\right)\Big|_{N=cte}} = \sqrt{\frac{1}{m}\frac{\partial}{\partial \rho}\left(\rho^2 \frac{\partial (E/N)}{\partial \rho}\right)} \\ &= \sqrt{\frac{1}{m}\left(2\rho \frac{\partial \left(E/N\right)}{\partial \rho} + \rho^2 \frac{\partial^2 \left(E/N\right)}{\partial \rho^2}\right)} \end{aligned} \tag{4.26}$$

On the other hand, the low momentum-momentum behaviour of the static structure factor is governed by phonons.

$$\begin{aligned} &\lim_{k\to 0} S_k = \lim_{k\to 0}\left[\Theta\left(k - 2k_F\right) + \frac{k}{2k_F}\left(\Pi\left[\frac{k}{2k_F} - \frac{1}{2}\right]\right)\right] = \lim_{k\to 0}\left(\frac{k}{2k_F}\right) = \lim_{k\to 0}\left(\frac{k\hbar}{2v_F m}\right) \\ &\Longrightarrow c = v_F = \frac{\hbar}{2m \cdot lim_{k\to 0}\left(\frac{S_k}{k}\right)} = \frac{\hbar}{2m}\left(\frac{dS_k}{dk}\right)^{-1}\Big|_{k=0} \end{aligned} \tag{4.27}$$

To summarize, we will use two complementary and independent methods to calculate the Luttinger parameter K.

$$K = \begin{cases} \pi\left(\dfrac{2}{\rho\epsilon_o}\dfrac{\partial(E/N)}{\partial\rho} + \dfrac{1}{\epsilon_o}\dfrac{\partial^2(E/N)}{\partial\rho^2}\right)^{-1/2} & \text{in reduced units} \\ 2\pi\rho\left.\dfrac{dS_k}{dk}\right|_{k=0} \end{cases} \tag{4.28}$$

In the frame of Luttinger liquid theory, this universal parameter defines long-range properties of correlation functions. The decay of the pair correlation function contains a monotonic K/x^2 part as well as oscillation terms of faster decay.

$$g(x) = 1 - \frac{K}{2\left(k_F x\right)^2} + \sum_{\ell=1}^{\infty} A_\ell \frac{\cos\left(2\ell k_F x\right)}{\left|k_F x\right|^{2\ell^2 K}} \tag{4.29}$$

It is important to note the amplitude A_ℓ of the oscillating terms cannot be calculated within the Luttinger liquid theory, and a priori it is not clear if the smooth decay in eq. (4.28) will dominate over the oscillating terms.

The Luttinger parameter is also related to the height of the ℓ-th peak in the static structure factor

$$S(k = 2\ell k_F) = A_\ell N^{1-2\ell^2 K} \tag{4.30}$$

From this equation we can see that the first peak will diverge for values of $K < 0.5$, and so we can consider that this is the limit for a crystal or "quasi-crystal" regime.

4.3.4 Phonon regime and healing length

We have constructed our guiding wave function as a piecewise function, where two regimes are matched: the particle regime (for small distances) and the phononic regime (for large distances). We have to recall that the scattering solution will be accurate for low densities since it only takes into account the two-body correlations while at high densities the phononic approach will be more suitable. The parameter R_{par} has indeed a physical meaning being of the order of the healing length ξ, that is the interatomic average distance where the energy per particle of the phonon mode and the energy of the free particle mode match:

$$\begin{aligned} \epsilon_{phonon} = \epsilon_{particle} \longrightarrow cp = \frac{p^2}{2m} + mc^2 \rightarrow \xi^2 - \frac{\hbar^2}{mc}\xi + \frac{\hbar^2}{2m^2c^2} = 0 \\ \xi = \frac{1}{\sqrt{2}}\frac{\hbar}{mc} \end{aligned} \tag{4.31}$$

Alternatively, the healing length can also be expressed in terms of the universal Luttinger parameter $K = K(\rho)$.

$$\xi = \frac{\hbar}{m\sqrt{2}}\frac{Km}{\hbar\pi\rho} \Longrightarrow \frac{K}{\xi} = \sqrt{2}\pi\rho \tag{4.32}$$

4.4 The Scattering problem for H-H potential

The solution of the scattering problem for hydrogen will be required for the construction of the trial wave function in a Jastrow form. We have constructed the Jastrow wave function as a piecewise-defined function

$$f_2(x) = \begin{cases} f_{tbs} & x < R_{par} \\ \left|\sin\left(\frac{\pi x}{L}\right)\right|^{1/K_{par}} & x > R_{par} \end{cases} \tag{4.33}$$

In order to obtain f_2 we need to solve the Schrödinger equation for $f_{tbs} \equiv f$ with the Hydrogen interaction and with the desired boundary conditions. On one hand we need to

impose continuity in the function and its derivative at the matching distance $x = R_{par}$ and on the other hand we need the function derivative to be zero at the origin since $f(x) = \pm f(-x)$. In summary, the problem is to solve

$$-\frac{\hbar^2}{2\mu}\frac{\partial^2 f(x)}{\partial x^2} + V\left(|x|\right) f(x) = \epsilon f(x) \tag{4.34}$$

with

$$f'(0) = 0, \qquad f(R_{par}) = \left|\sin\left(\frac{\pi R_{par}}{L}\right)\right|^{1/K_{par}}, \qquad f'(R_{par}) = \left(\frac{\pi}{K_{par}L}\right)\left(\frac{\cos\left(\frac{\pi R_{par}}{L}\right)}{\left(\sin\left(\frac{\pi R_{par}}{L}\right)\right)^{\frac{1}{K_{par}}-1}}\right) \tag{4.35}$$

Since we will solve the problem with periodic boundary conditions with a box of size L, we will find the ground state scattering wave-function in the interval $0 \to L/2$. We also have to recall that the scattering energy is a parameter that must be tunned in order to fulfill the boundary conditions (so the problem is not overdetermined).

Equation (4.34) can be solved numerically using a finite difference method and a shooting algorithm in order to find the ground state solution, which for this potential will be an unbound state with no nodes (since the depth of the potential well is not large enough to produce bound states), that fulfills the condition at 0 that is equivalent to $\Psi(0) = 0$ since the strength of the potential interaction near the origin.

We can ensure that the wave function $f_2(x)$ and its first derivative will be continuous, however the second derivative, and so the local energy, are not always going to be continuous (depending on the parameters R_{par} and K_{par}). In figure 4.5 we show an example of the problem solved for tritium at $\rho = 0.3\mathring{A}^{-1}$ and for $N = 10$ particles per box, at the parameters $R_{par} = L/2$ and $K_{par} = 1$

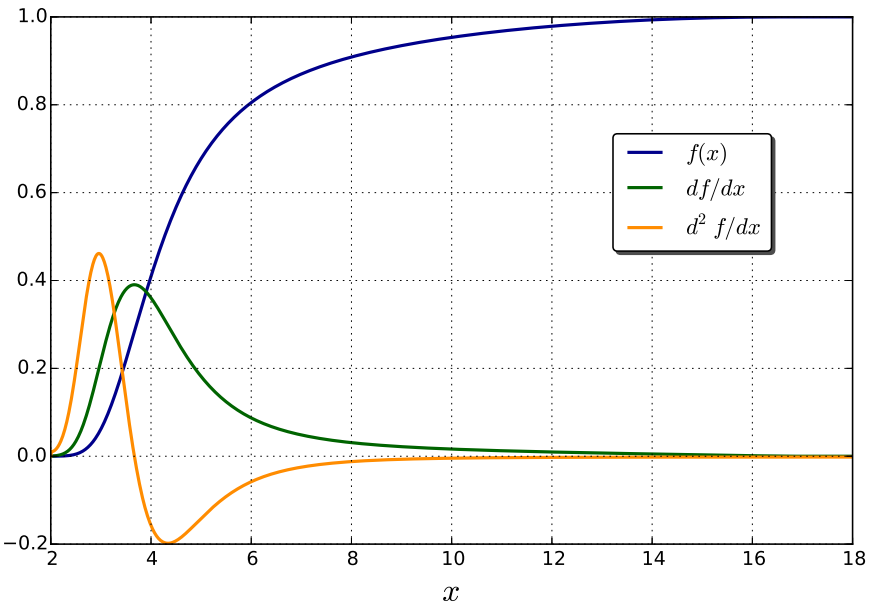

Figure 4.5: Two-body scattering solution and derivatives

We can see here the fulfillment of the boundary conditions and also the continuity in the derivatives. In this case, we choose $f_2(x) \equiv f_{tbp}(x)$ and so no matching point exists and no possibility of the second derivative discontinuity.

5. *Results*

The problem stated in the previous Chapter has been solved employing the two Monte Carlo methods described in Section 3.1, VMC and DMC. In the following we present a summary of the variational results and we analyse in detail the results obtained with DMC method.

5.1 Variational Results

Here we present the results obtained from the variational code we developed. We have to take into account that these results provide an upper bound for the ground state energy, while the exact results will be obtained from the difussion method. Here we report the variational energy, the static structure factor, the pair distribution functions, the static structure factor and the Luttinger parameter K in terms of the density. The data has been computed for the three species, hydrogen, deuterium and tritium and for densities ranging from $0.001\mathring{A}^{-1}$ to $0.3\mathring{A}^{-1}$

5.1.1 Energy

As we can see in figure 5.1, at low densities we recover the ρ^2 dependence, typically for an ideal Fermi gas. At large densities the repulsive part of the potential at short distances make the system more rigid suggesting the formation of a crystal. For intermediate densities the attractive part of the potential plays an important role contributing to the total energy and so the energy of the system proves to be lower than in an ideal Fermi gas. The effect of this attractive part of the potential is more important for tritium while for hydrogen and deuterium has a little effect, being hydrogen very close to an ideal Fermi gas for a wide range of low densities. We have to recall that the true g.s. energy of the system is smaller than that obtained in a variational approach and will be reported in Chapter 5.2, where DMC results will be presented.

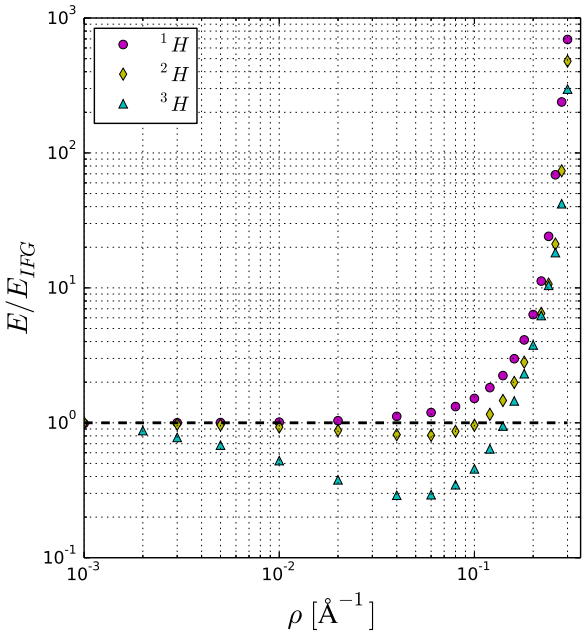

Figure 5.1: Variational ground-state energy in double logarithmic axes. The energy is normalized respect to the energy ot the IFG, $E_{IFG} = \frac{\pi^2\rho^2}{6m}$.

5.1.2 Static Structure Factor

The static structure factor is computed from the Fourier transform of the pair distribution function and is reported in figures 5.2, 5.3 and 5.4 in terms of the Fermi momentum. We show separately the three species for different densities.

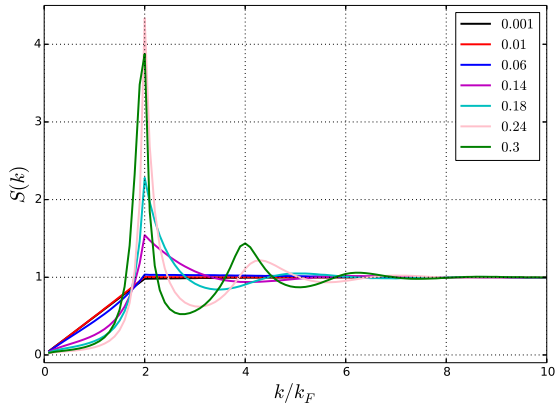

Figure 5.2: Hydrogen

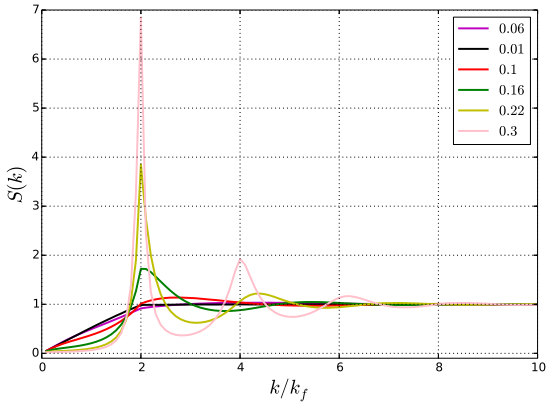

Figure 5.3: Deuterium

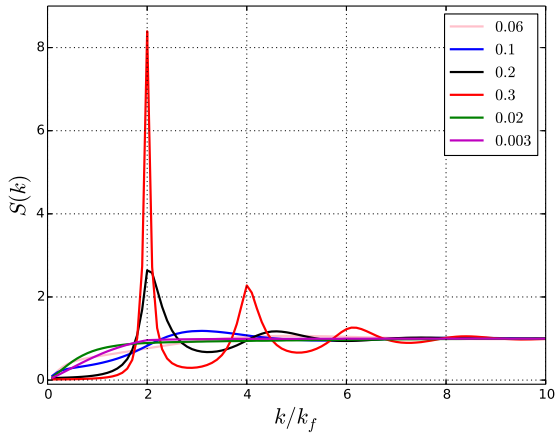

Figure 5.4: Tritium

The static structure factor yields information about spatial order in the system. The presence of diverging peaks suggests a formation of a quasi-crystal in the system. Then, we see that for large densities the three species end up forming a quasi-crystal, however the crystal starts its formation at a lower density for the tritium isotope. For densities bigger than $0.3\mathring{A}^{-1}$ the quasi-crystal can be considered as a formed one.

At low enough densities the system exhibits the behaviour of the non-interacting gas, with a linear dependence up to $k = 2k_F$ and a constant and equal to one for larger momenta. The linear behaviour of $S(k)$ at low momentum makes it possible to relate the slope to the speed of sound, according to eq. (4.27).

5.1.3 Luttinger Parameter K

The Luttinger parameter is computed from the speed of sound extracted from $S(k)$ and can be useful in order to differentiate between the three regimes: Bose gas, super Tonks-Girardeu and quasi-crystal.

The different regimes are defined by the value of K. For values higher than one the system is in a Bose gas regime, for values between 0.5 and 1 the system is in a super Tonks-Girardeau sTG regime and for lower values we have a quasi-crystal. Then we can see again that the richer specie is tritium in which we find a wider range of the Luttinger parameter K. Also we find that it is the first isotope to form the quasi-crystal.

For the hydrogen system we see that the main regime is the sTG due to the insignificant contribution of the attractive part of the potential, so that the repulsive interaction dominates the physics of the system.

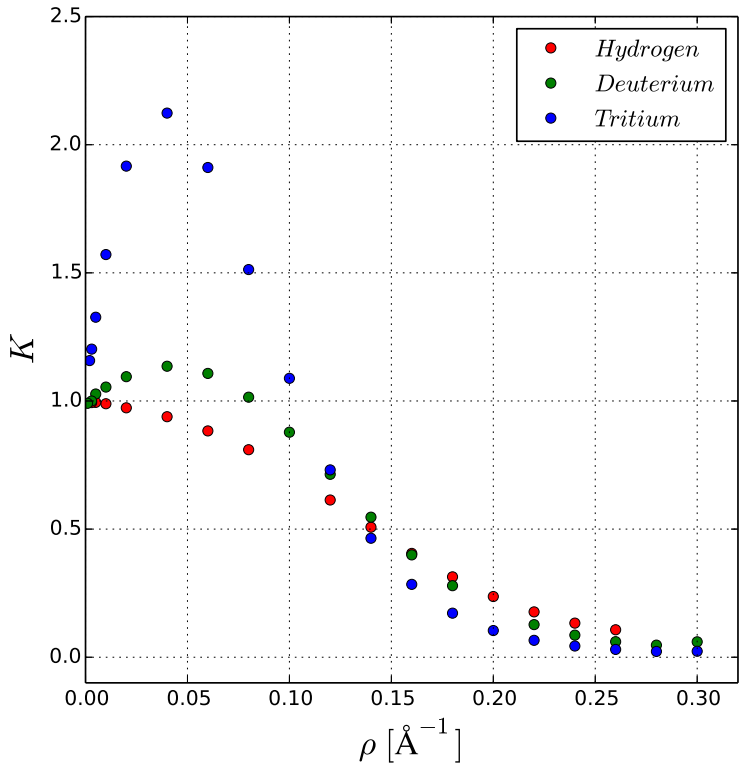

Figure 5.5: Luttinger parameter.

5.1.4 Optimization

The optimization of the wave function with a large number of parameters is in general a difficult task. However in our case we only have two parameters K_{par} and R_{par}, and its optimization can be carried out in a simple way. We find that the energy has a weak dependence on K_{par} while has a relevant dependence in R_{par}. In order to find a suitable optimized guide function for the DMC method, we find the R_{par} that minimizes the energy and employ the parameter K_{par} found with DMC. However the trial wave function with $R_{par} = L/2$ proves to be good enough for small densities, since in this case we recover the IFG limit with $K = 1$ and so the two-body solution reproduces the phononic one.

Figure 5.6 shows an example for the energy in terms of R_{par} for deuterium at $\rho = 0.22\mathring{A}^{-1}$. Close to its minimum, the energy can be well approximated with a quadratic fit $E/N(R_{par}) = a(x-b)^2 + c$

We also show in figure 5.7 the parameter R_{par} for which the energy is minimized in terms of the density.

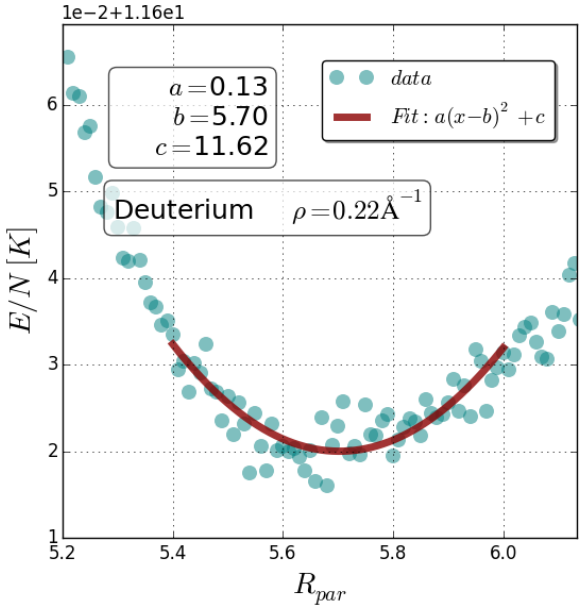

Figure 5.6: Energy minimization in VMC. Here R_{par} is expressed in $\mathring{A}$.

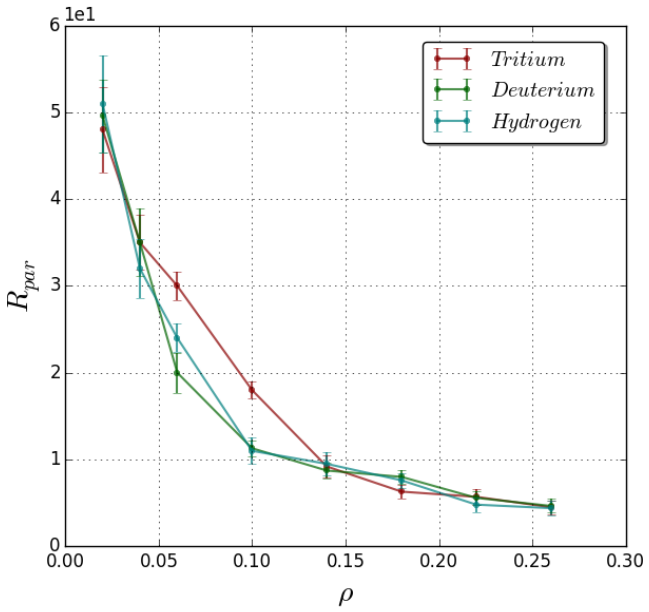

Figure 5.7: Variations parameter R_{par}. Here ρ is expressed in $\mathring{A}^{-1}$.

5.2 DMC Results

In this section we report the results obtained with the DMC method. The quantities $g(r)$, $S(k)$ and $K(\rho)$ shown here are computed using the extrapolation technique, in order to obtain an approximation to the pure estimator.

5.2.1 Energy

The DMC method is very precise in calculating the ground-state energy of the system. We performed a detailed study of the statistical errors, number of walkers and the time-step. In the following graph we show the energy of the three isotopes in the same figure

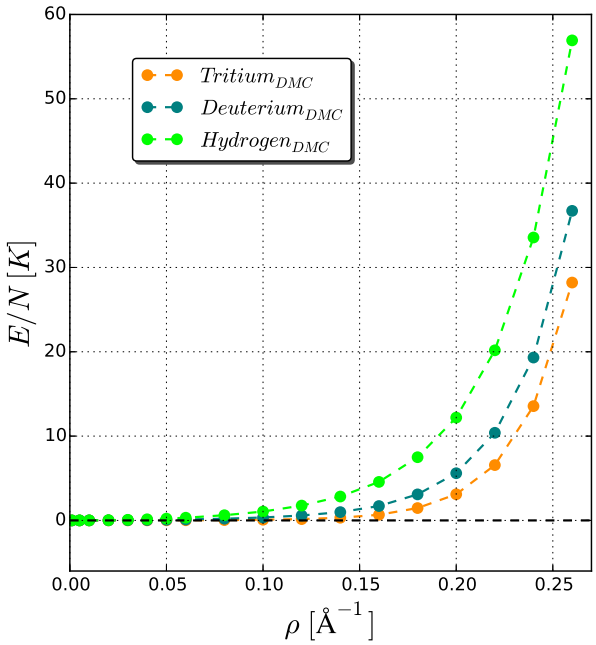

Figure 5.8: DMC energy in a linear scale

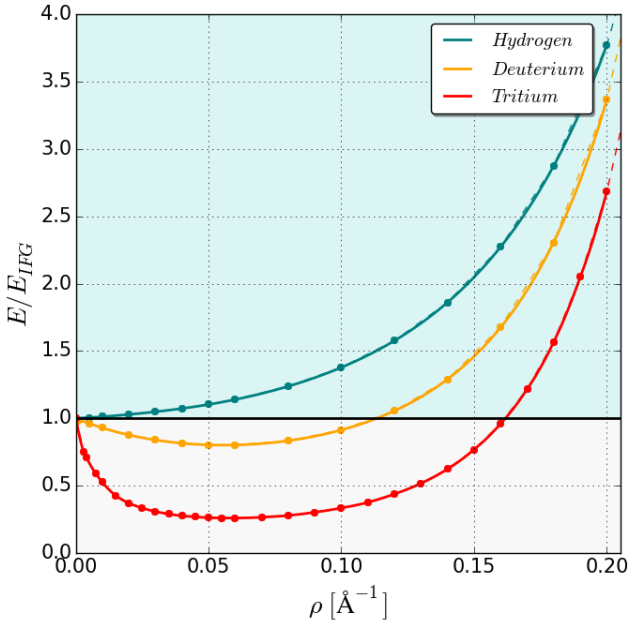

Figure 5.9: DMC energy in units of the IFG energy.

We see that no one of the hydrogen isotopes present a inflexion in the state equation, so there is not a liquid phase in any of the isotopes in one dimension. We find that for the same density the largest energy is that of the hydrogen, followed by deuterium and being tritium the one with the lowest energy. The reason for that is the zero-point oscillations, which are largest for the smallest mass.

It is also interesting to compare the energy result obtained from DMC and VMC, and also compare it with the Fermi energy that must be the limit for low densities.

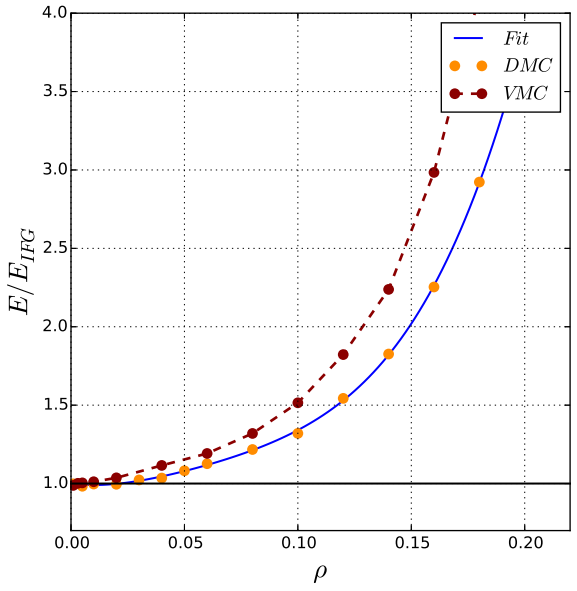

Figure 5.10: Energy VMC vs DMC for Hydrogen

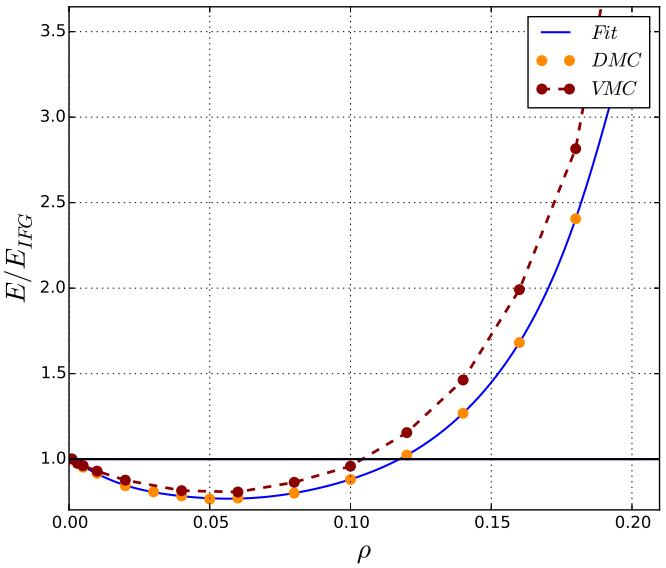

Figure 5.11: Energy VMC vs DMC for Deuterium

Indeed, we find that the difference between VMC and DMC energy is very small, proving a very good quality of the guiding wave function.

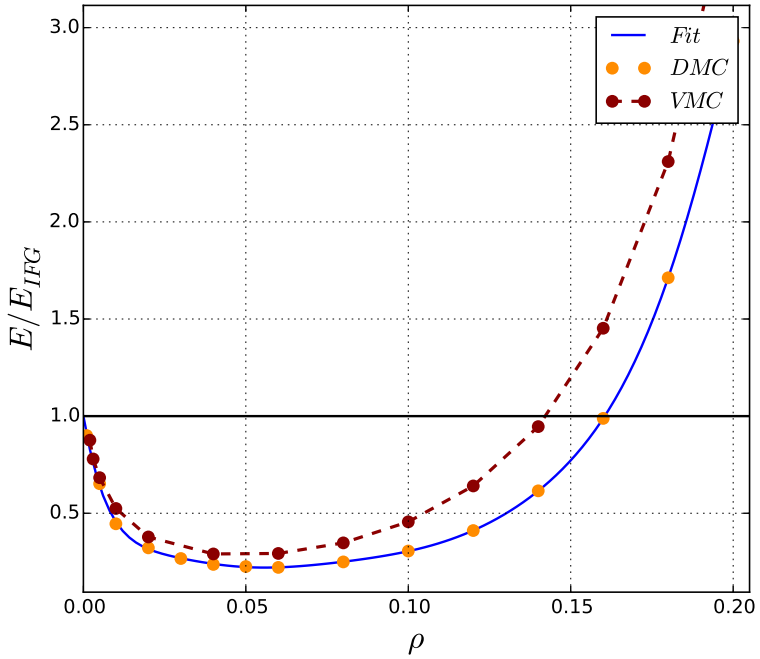

Figure 5.12: Energy VMC vs DMC for Tritium

We fit the DMC energy with a polynomial expansion

$$\frac{E}{N} = \frac{\pi^2\hbar^2\rho^2}{6m}\left(1 + \sum_{i=1}^{n} a_i \rho^i\right) \tag{5.1}$$

where the coefficients in units of $[a_i] = \text{Å}^{\,i}$ are collected in the following table

	Hydrogen	Deuterium	Tritium
a_1	$9.51 \cdot 10^{-1}$	$-7.96 \cdot 10^{0}$	$-8.07 \cdot 10^{1}$
a_2	$2.04 \cdot 10^{1}$	$8.43 \cdot 10^{1}$	$3.43 \cdot 10^{3}$
a_3	$-2.06 \cdot 10^{1}$	$2.79 \cdot 10^{2}$	$-7.43 \cdot 10^{4}$
a_4	$1.01 \cdot 10^{3}$	$-1.24 \cdot 10^{4}$	$8.81 \cdot 10^{5}$
a_5	$5.64 \cdot 10^{2}$	$1.29 \cdot 10^{5}$	$-5.74 \cdot 10^{6}$
a_6	$-2.00 \cdot 10^{4}$	$-5.70 \cdot 10^{5}$	$1.93 \cdot 10^{7}$
a_7	$1.11 \cdot 10^{5}$	$1.05 \cdot 10^{6}$	$-2.59 \cdot 10^{7}$

With this polynomial expansion we have seen the behaviour of our systems at low densities and we can also observe that, at low densities, hydrogen is the one closer to the ideal Fermi gas, fact that is reflected in the a_1 coefficient that is the lowest of the three.

Hydrogen interaction potential is valid for distances larger than 0.5Å or energies lower than $1.2{\cdot}10^5$ K, however the data we have for the potential presents irregularities in the derivatives in the potential wall for distances smaller than 2Å. We trust the results for densities lower than 0.5Å^{-1}. We see that at high densities the major contribution of the energy is the potential energy as we expect since the atoms are localized around the equilibrium positions.

The energy of the isotopes approaches to that of the classical harmonic crystal, being very close at densities higher than 0.3Å^{-1}.

The following plot reflects the energy diagram for a wide range of densities, summarizing main ideas expressed above. Here we have plotted the two limits: for high densities the Harmonic crystal energy and for low densities the the ideal Fermi gas energy as solid lines.

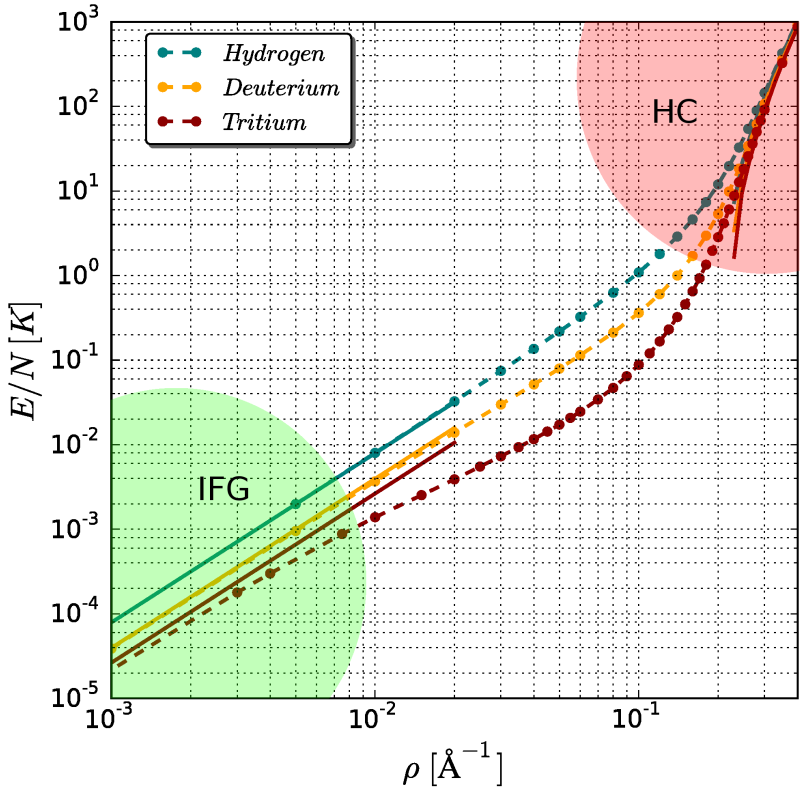

Figure 5.13: Wide density range energy plot. The energy of the three isotopes is drawn in dashed lines. The solid lines at low densities show the ideal Fermi gas energy. The solid lines at high densities show the classical harmonic crystal energy.

Since the energy for high densities fits accurately to the one of the Harmonic crystal, the energy can be computed directly from the potential following (2.55)

Error in DMC Energy

In order to have an idea of the robustness of the method ans so the confidence of the obtained results, in this case for the energy, it is convenient to study the energy dependence on the number of walkers, on the time step and on the number of particles. Then we can estimate the error due to the different sources of error.

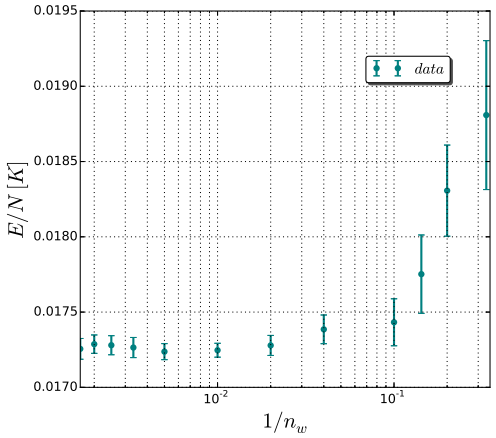

Figure 5.14: Energy in terms of the number of walkers

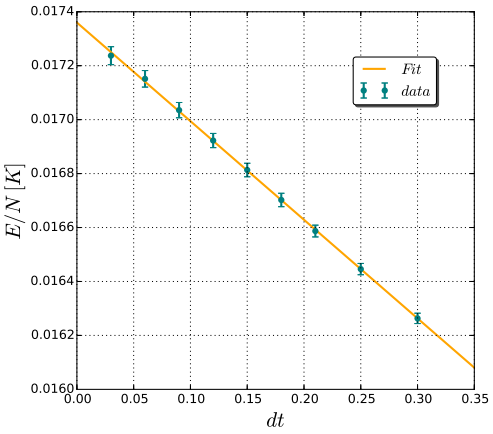

Figure 5.15: Energy dependence with the time step

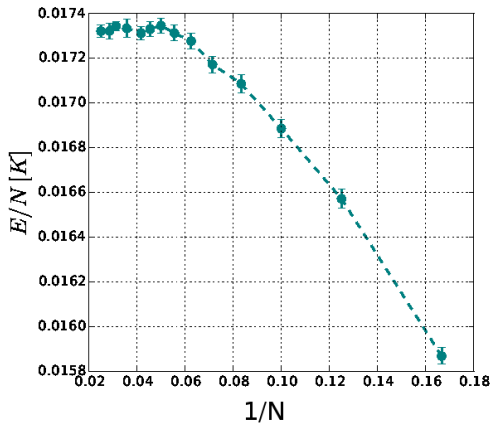

Figure 5.16: Energy dependence with the number of particles in the box

So we can see that in this case, for a density $\rho = 0.05\mathring{A}^{-1}$ and for tritium, the dependence of the energy with the number of particles, with the time step and with the number of walkers are consistent and tend to a value of $E/N \sim 0.1739K$. We can also see that the selected values in our calculations are suitable, in this case the time-step $dt = 0.03$, the number of walkers $n_w = 200$ and the number of particles $n_p = 20$.

5.2.2 Pair Correlation Function

Here we discuss the result of the calculation of the pair correlation function from the DMC code. In the following images we show the results for different densities. In the plots in the following page, the x-axis of the radial distribution functions are normalized with the density and so the peaks appear at integer numbers. The formation of strong peaks suggest the presence of a pseudo crystal for densities bigger than 0.14Å^{-1}. Following the idea of an ideal crystal the peaks in $g(r)$ tend to decrease its width while increasing its height when increasing the density, approaching the delta distribution.

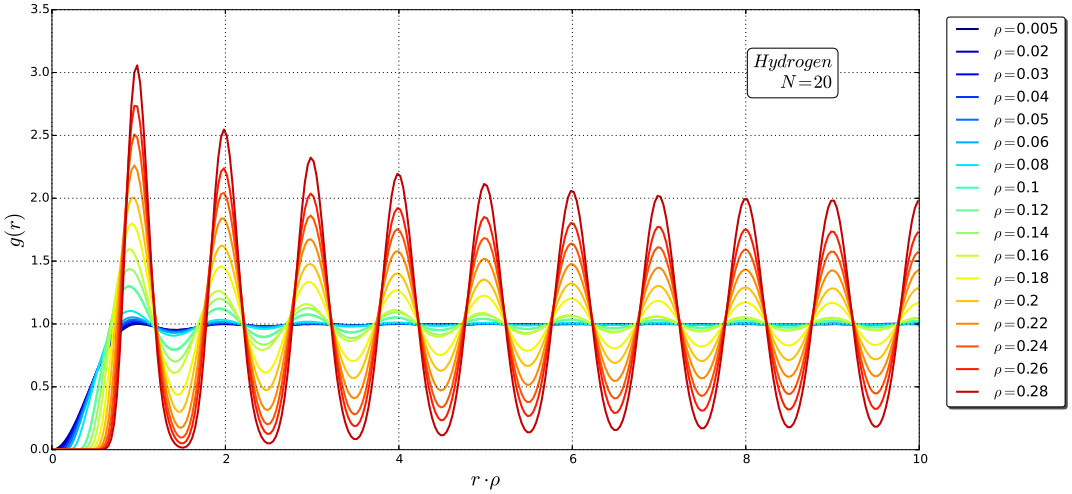

Figure 5.17: Pair correlation functions for hydrogen for a wide range of densities.

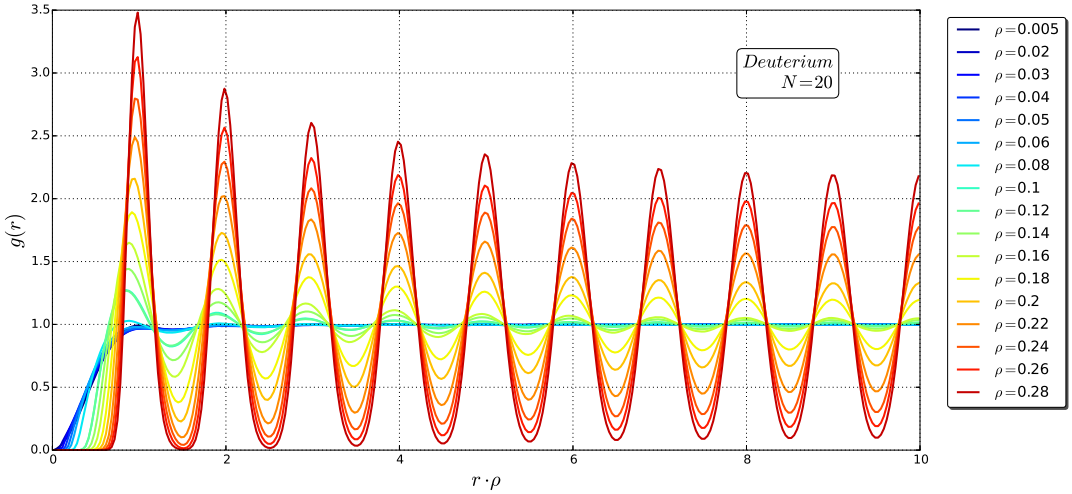

Figure 5.18: Pair correlation functions for deuterium for a wide range of densities.

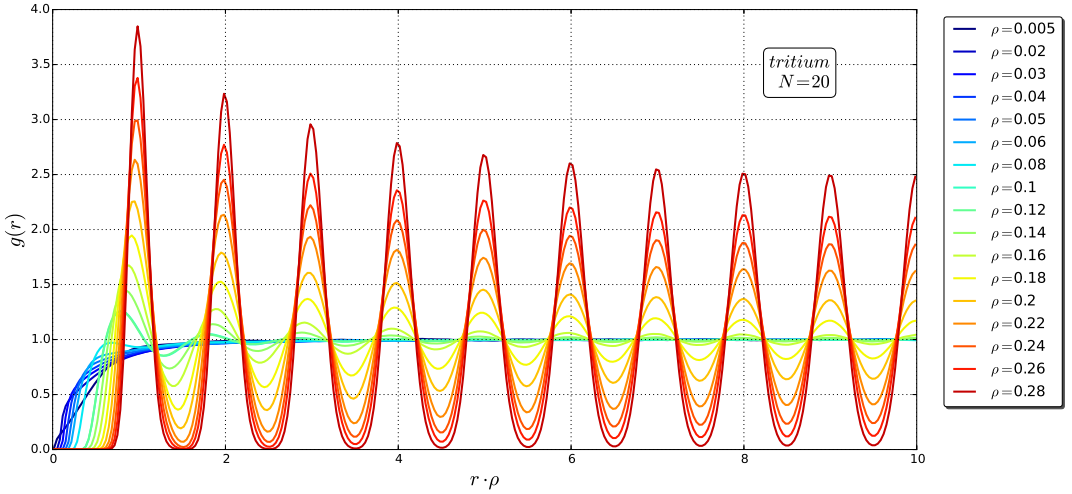

Figure 5.19: Pair correlation functions for tritium for a wide range of densities.

The next combined plot reflect another key idea that is that, as we expected, the first peak

of the radial distribution function moves to the left when increasing the density, it is that the atoms tend to approach the potential barrier following the law of $x = 1/\rho$ in order to minimize the energy of the system. For low densities, the atoms remain far away from the potential wall.

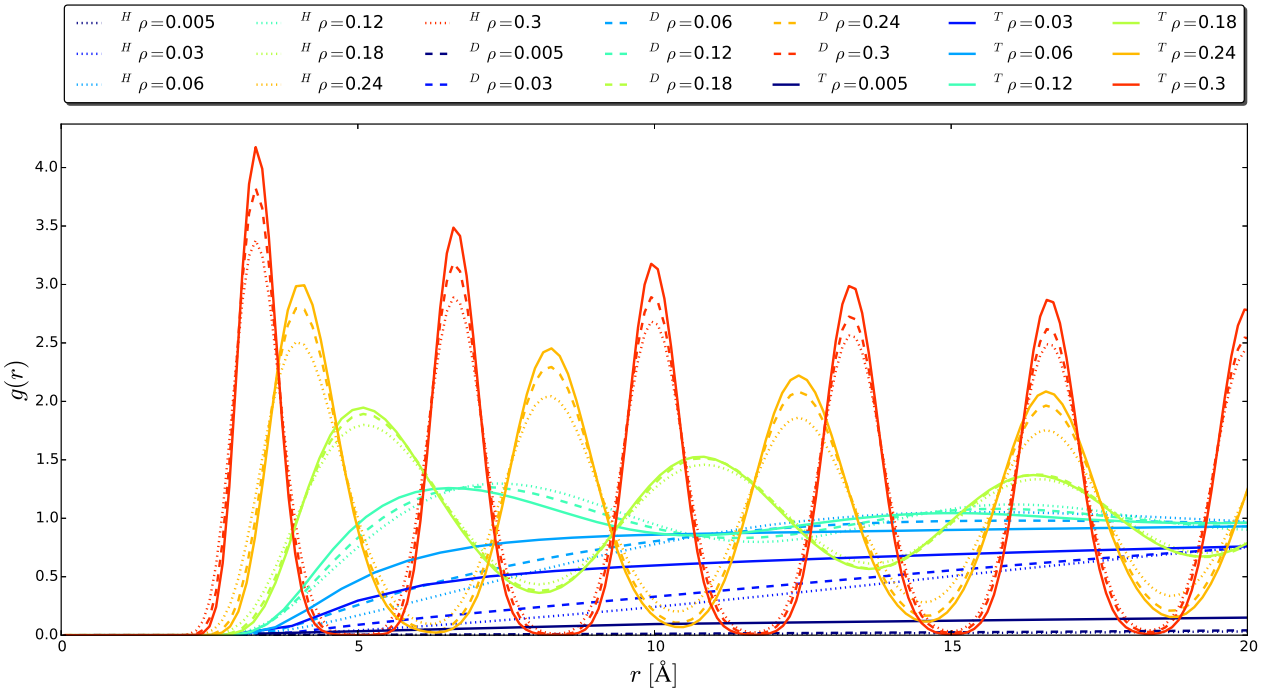

Figure 5.20: Pair correlation function comparison.

The following three detailed plots show the first peak of the $g(r)$. It's interesting to note how the position of the first peak does not deviate from the one of the ideal crystal $(1/\rho)$ while increasing the density. This is de desired behaviour for our crystal

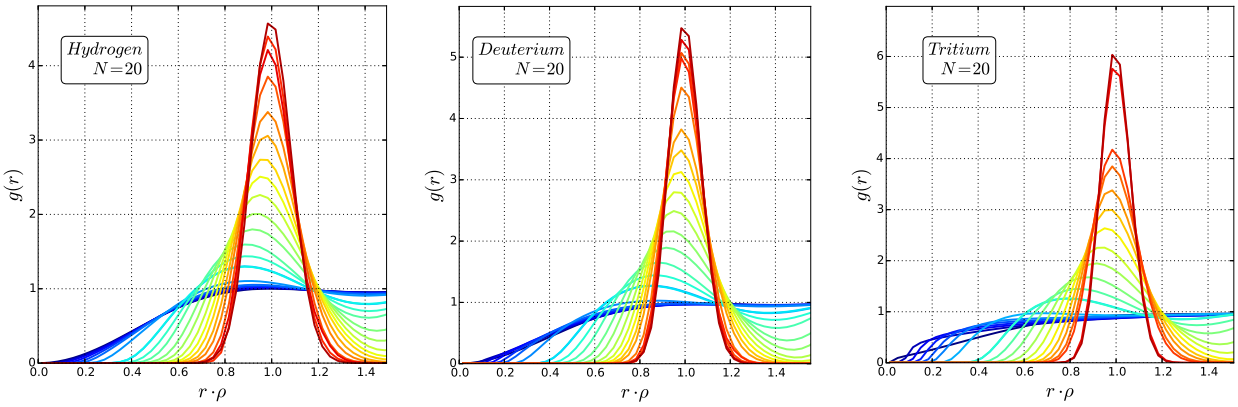

Figure 5.21: Pair correlation detail. The peaks of $g(r)$ grow increasing the density.

Even more we can verify that the peaks of $g(r)$ for large values of ρ follow a normalized Gaussian distribution, as we can see in the following fit for densities of $\rho = 0.3\mathring{A}^{-1}$ and $\rho = 0.7\mathring{A}^{-1}$ in the case of tritium

Mathematically we can see the delta distribution as the limit of a Gaussian distribution. It

is

$$\delta(x-\mu) = \lim_{\sigma \to 0} \quad \frac{1}{\sigma\sqrt{2\pi}} exp\left(-\frac{1}{2}\left(\frac{x-\mu}{\sigma}\right)^2\right) \tag{5.2}$$

and since $\sigma(\rho) \to 0$ when $\rho \to \infty$, the distribution approaches the one of an ideal crystal, as it was said.

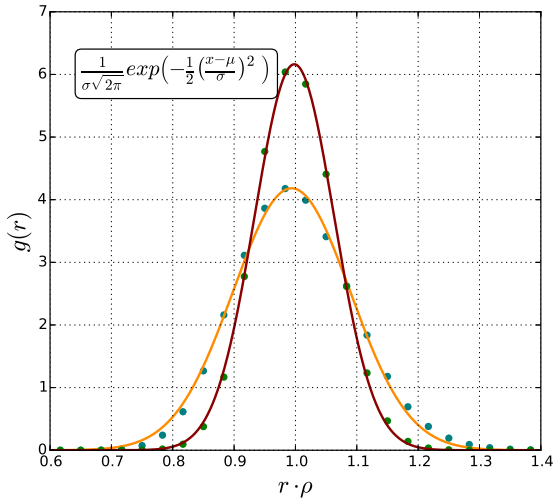

Figure 5.22: Gaussian shape of $g(r)$ for large densities. We show the data in dots and the fit to a Gaussian distribution in solid line. Both curves represent different densities for tritium. The red line corresponds to $\rho = 0.7\text{Å}^{-1}$. The orange line corresponds to $\rho = 0.3\text{Å}^{-1}$

We calculate the pair distribution function (RDF) of the three isotopes for low densities (but not too low) and compare it with the one of the ideal Fermi gas. In the following graphs we show the RDF for $\rho = 0.02\mathring{A}^{-1}$ (left) ad for $\rho = 0.05\mathring{A}^{-1}$ (right). We see that for this densities Hydrogen and Deuterium exhibit a behaviour very close to the IFG with a very slight variations , being deuterium at $\rho = 0.05\mathring{A}^{-1}$ a little bit closer to a Bose gas and hydrogen closer to a hard-rod gas. On the other side, tritium shows a very different appearance, being closer to what is similar to a weakly interacting Bose gas in the sense that it has the corresponding value of the Luttinger parameter.

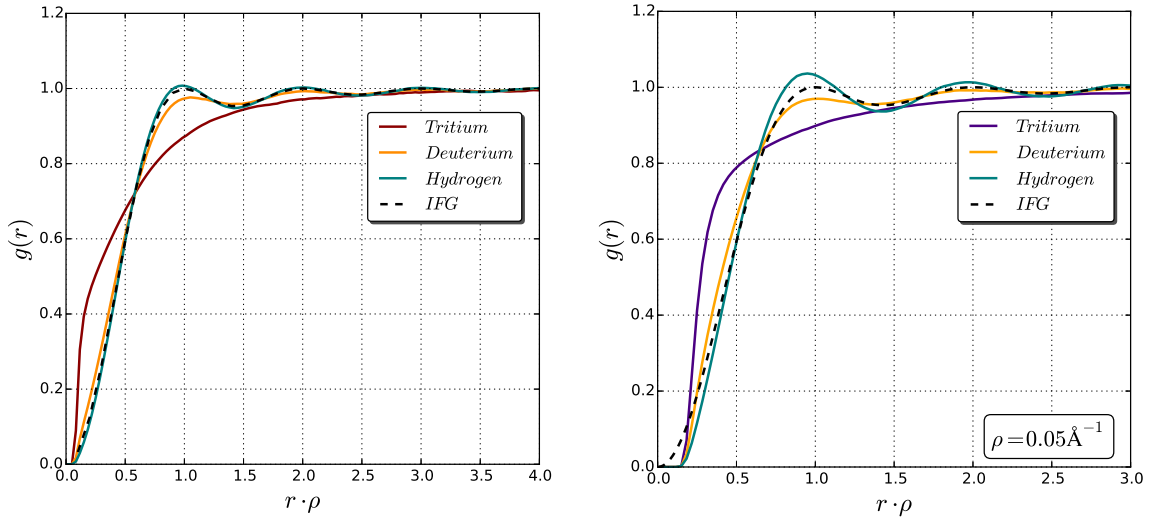

Figure 5.23: Two body correlation function detail for small densities. $\rho = 0.02\text{Å}^{-1}$ at left. $\rho = 0.05\text{Å}^{-1}$ at right.

Also, the $g(r)$ for tritium is a continuous function which smoothly approaches is large-distance asymptotic value. This behaviour is typically for a weakly interacting Bose gas. On the contrary, hydrogen and deuterium show Friedel oscillations typical for an IFG.

For low enough densities all the isotopes show the ideal behaviour of the IFG, as we should expect. We can also verify that the different pair correlation functions are proportional to the square of the two body scattering function for short distances.

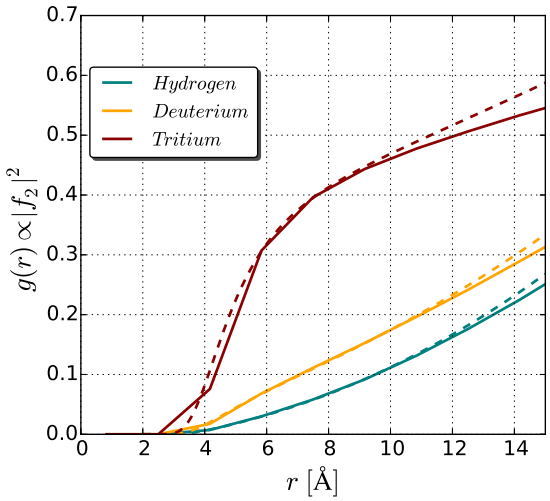

Figure 5.24: Comparison between $g(r)$ (solid line) and $|f_2|^2$ (dashed line) adjusting the proportional factor related to the *contact* ,C, for a density of $\rho = 0.02\text{Å}^{-1}$. For ^{1}H, $\mathcal{C} \sim 2.58$; for ^{2}H, $\mathcal{C} \sim 2.40$; and for ^{3}H, $\mathcal{C} \sim 1.94$ in units of ρ^{-1}, taking into account a $|f_2|^2$ defined as in 4.3.2.

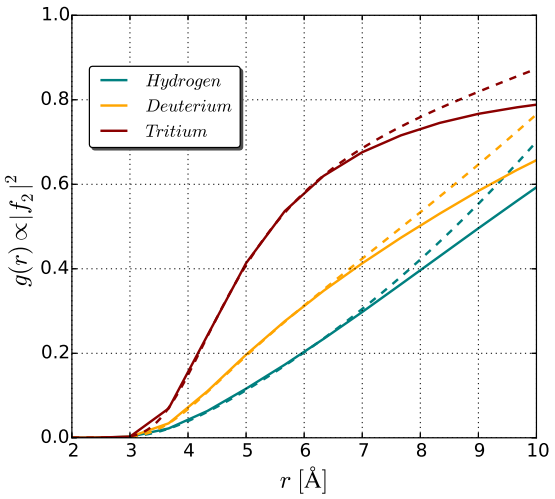

Figure 5.25: Comparison between $g(r)$ (solid line) and $|f_2|^2$ (dashed line) adjusting the proportional factor related to the *contact* ,C, for a density of $\rho = 0.05\text{Å}^{-1}$. For ^{1}H, $\mathcal{C} \sim 6.25$; for ^{2}H, $\mathcal{C} \sim 4.75$; and for ^{3}H, $\mathcal{C} \sim 2.65$ in units of ρ^{-1}, taking into account a $|f_2|^2$ defined as in 4.3.2.

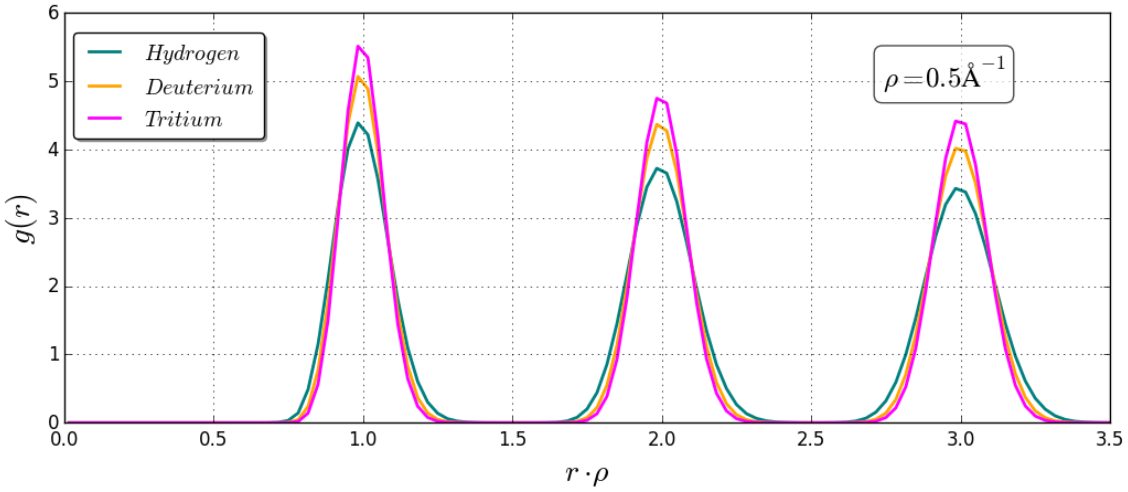

Figure 5.26: Detail of g(r) for large densities. Comparison between the isotopes.

As it can be seen in figure 5.25, the atoms at high densities are localized around the multiples of ρ^{-1} and show a Gaussian shape. However, what is interesting about this figure is to notice

the role of the mass in the characteristics of the crystal. Here we can see that Hydrogen is the one that exhibits a higher degree of delocalization around the equilibrium points due to its low mass that allows the atoms to move faster (in a classical sense). On the contrary, the distribution of tritium is the closest to the delta distribution since its higher mass limits the ability to move around the minimum energy points.

5.2.3 Static Structure Factor

Another important quantity is the static structure factor (SSF). We plot it for different densities for each isotope. We find that for low densities the shape of the SSF is close to the one of the IFG, specially for hydrogen. At high densities a diverging peak appears at $k = 2k_F$, suggesting the formation of a quasi-crystal. Increasing the density the number of peaks grows and it appears some more peaks at $k = 2nk_F$, where $n \in \mathbb{N}$.

The maximum intensity of this peak depends on the number of atoms in the system since the addition of a new atom contributes to the total height, not as in an ideal one-dimensional crystal ($S(2k_F) = N$) but in some power law involving the Luttinger parameter K, see 4.30. We have tested this relation for some densities and we find that the values obtained for K from this fit do not agree with the value obtained from energy and $S(k)$. Depending on the density, the value obtained differs about a 10%, that is too much.

The slopte of the static structure factor at low momenta has a nearly monotonous dependence on the density for hydrogen and deuterium, decreasing the slope of $S(k)$ when ρ increases. For tritium, the dependence of $S(k)$ on the density is not monotonous, increasing at low densities and decreasing for densities higher than $\rho = 0.05\mathring{A}^{-1}$. This behaviour is reflected in the Luttinger parameter.

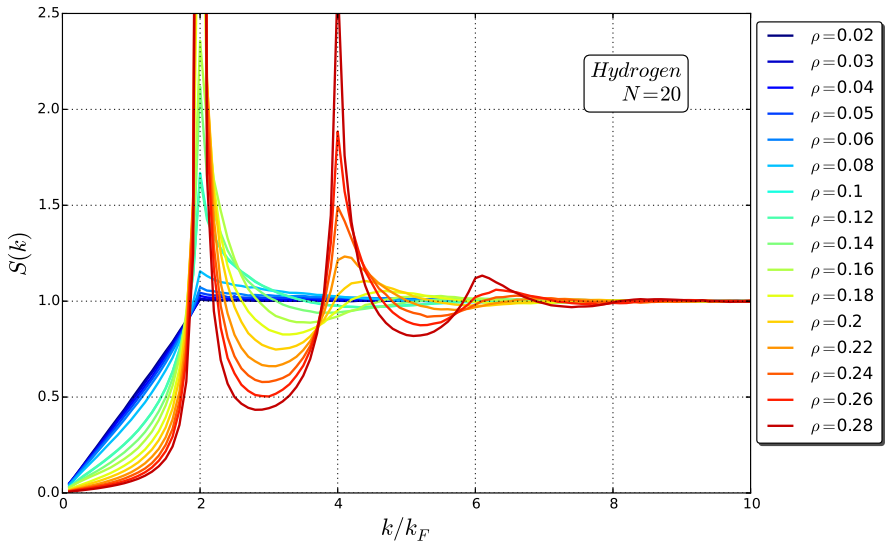

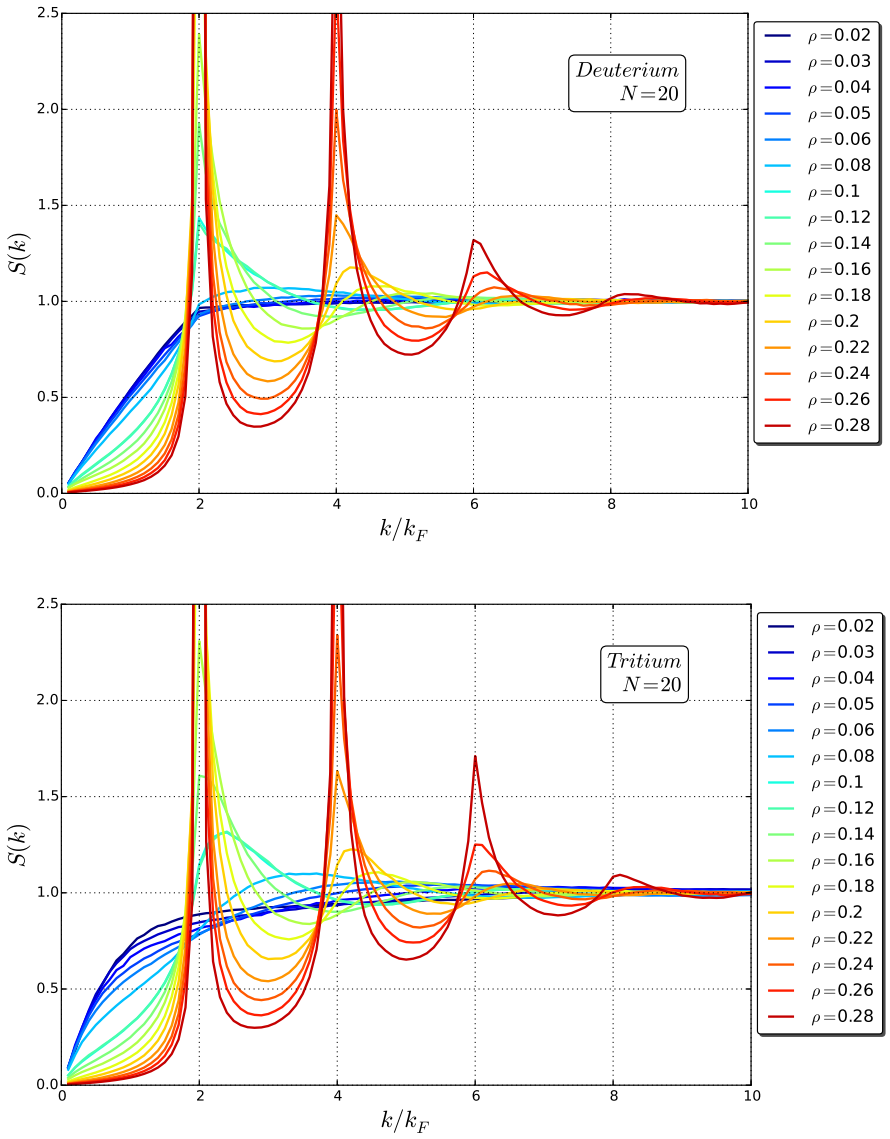

Figure 5.27: $S(k)$ for hydrogen deuterium and tritium.

5.2.4 Luttinger parameter

While in the variational-computed Luttinger parameters we can only have an approximation to the behaviour of our systems, now we have a good estimator of the parameter that is exact at first order making use of the extrapolated estimator for $S(k)$. Even more, we can compute the Luttinger parameter from the energy and so obtain a better approach since DMC technique is exact in energy. In order to validate our results it would be convenient to check a coincidence between both ways of computing K, since both methods are totally different and an agreement here would be a non-trivial desirable result.

In the figure 5.2.4 we show the parameter K in terms of ρ computed in both ways, see Eq. 4.28. Despite we find some discrepancies in $K(\rho)$ the result is quite good. A small deviation in the results may be consequence of the discretization in $S(k)$ due to the finite number of particles in the simulation box. Due to the poor accuracy of the fit that a polynomial

gives for the tritium energy at low densities, the sensitivity in the derivatives makes the computation of the Luttinger parameter not suitable. Here we make an spline of order 3 of the energy and we compute numerically the Luttinger parameter, fitting it once computed in order to smooth the curve. The three regimes (Bose Gas, super Tonks-Girardeau and quasi-crystal regime) from Luttinger theory are depicted and labelled. Solid lines are computed from the derivatives of the polynomial fit of the energy and the dots are computed directly from the static structure factor.

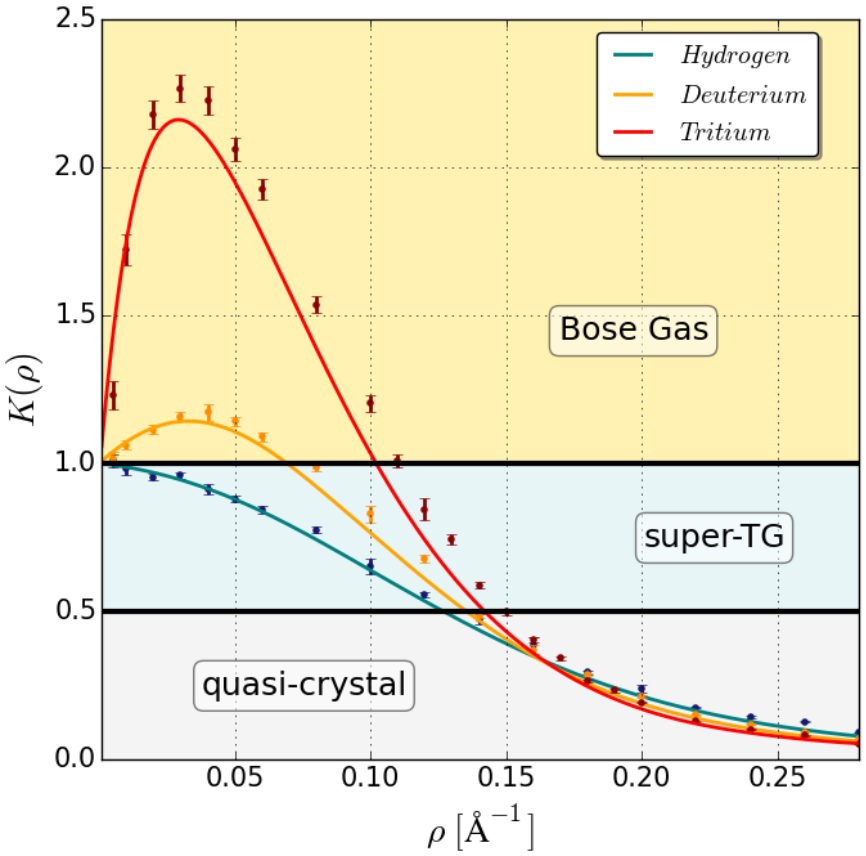

Figure 5.28: Luttinger parameter K for the different isotopes.

So we can conclude that Hydrogen does not exhibit Bose-gas behaviour while deuterium presents a weak Bose gas range up to $\rho \sim 0.07\mathring{A}^{-1}$ and tritium shows a clear example of Bose gas up to $\rho \sim 0.11\mathring{A}^{-1}$, with a maximum value of the Luttinger parameter $K \sim 2.5$. For higher densities they cross a super Tonks-girardeu regime and lately they become quasi-crystals.

6. *Conclusions*

We have studied the ground state properties of hydrogen, deuterium and tritium at zero-temperature. We find the equation of state and some local properties like the static structure factor or the pair correlation function.

The main idea we have to say is that while the statistics of the species (hydrogen and tritium bosons and deuterium a fermion) and the polarization do not affect the energy and local properties of the system (in this sense the 1D system is independent from the statistics), the mass is the crucial factor that controls the system behaviour. The mass plays a non-straightforward role making the three species intrinsically different, especially in the case of tritium which differs significantly from hydrogen and deuterium, the difference being maximum at densities around $0.05\mathring{A}^{-1}$. We observe different regimes: Bose gas, super Tonks-Girardeau (sTG) gas and quasi-crystal regime. The systems do not show liquid phase, as proven by the absence of inflection in EoS, due to the light mass of all the isotopes, however tritium is the closer one to the liquid phase.

At very low densities the three isotopes behave like an ideal Fermi gas (IFG). The energy of the different isotopes matches the energy of an IFG at densities close to zero; while we can consider that hydrogen and deuterium are close to the IFG for densities below $0.05\mathring{A}^{-1}$ (at this density $E_H \sim 1.2E_{IFG}$ and $E_D \sim 0.8E_{IFG}$), tritium differs ($E_T \sim 0.3E_{IFG}$) and can be considered close to the IFG only for densities below $0.005\mathring{A}-1$. The same can be observed from the radial distribution function (RDF), where hydrogen and deuterium are close to the RDF of the IFG ($g(x) = 1 - \mathrm{sinc}^2(k_f x)$) while tritium behaves like a repulsive Bose gas, without exhibiting oscillations (it is without localization or structure). In the same sense, tritium atoms tend to aggregate more, being the RDF closer to the potential wall than ^{1}H and ^{2}H. The static structure factor shows the same, being interesting to notice the behaviour for tritium, in which the slope of $S(k)$ in terms of the density first increases from the one of the IFG and then decreases for densities bigger than $0.03\mathring{A}^{-1}$.

When increasing the density, the three isotopes go over the STG regime corresponding to a Fermi system with dominant repulsion, with a $g(r)$ presenting oscillations for distances higher than the minimum of the potential, and with a $S(k)$ showing non diverging peaks. If we further increase the density, the systems approach the potential wall and the physics start to be dominated by the repulsive potential. The $g(r)$ shows the shape of a crystal, periodic with the atoms localized around the minimum energy positions, with a Gaussian shape of the peaks of $g(r)$ (this allows us to fit the energy of the system to the harmonic crystal model) that tends to a delta distribution for very high densities, and with a $S(k)$ showing diverging peaks at $k = 2nk_F$.

Appendices

A. *Testing DMC. Harmonic Oscillator.*

In order to verify the proper operation of the DMC code, it is useful to check our results against an exactly solvable system like the quantum harmonic oscillator (QHO). In the natural length and energy units, the Hamiltonian for the one dimensional QHO is

$$\tilde{H} = -\frac{1}{2}\frac{d^2}{d\tilde{x}^2} + \frac{1}{2}\tilde{x}^2; \qquad E = \tilde{E}\cdot(\hbar\omega) \quad x = \tilde{x}\cdot\left(\sqrt{\frac{\hbar}{m\omega}}\right) \tag{A.1}$$

The units of time (for the DMC algorithm) will be the inverse of the energy scale $\tau_o = 1/\hbar\omega$. First of all we have tested the results of the DMC code without importance sampling, that is without guiding wave function, or equivalently $\Psi_T = const$. In this case, the results is widely known: the DMC code is capable of giving the correct value of the energy ($E = 0.5\hbar\omega$) with a high precision, finding a probability distribution (it is a distribution of walkers) with a variance twice the one of the ground state exact function. The results of our test is summarized in figure A1

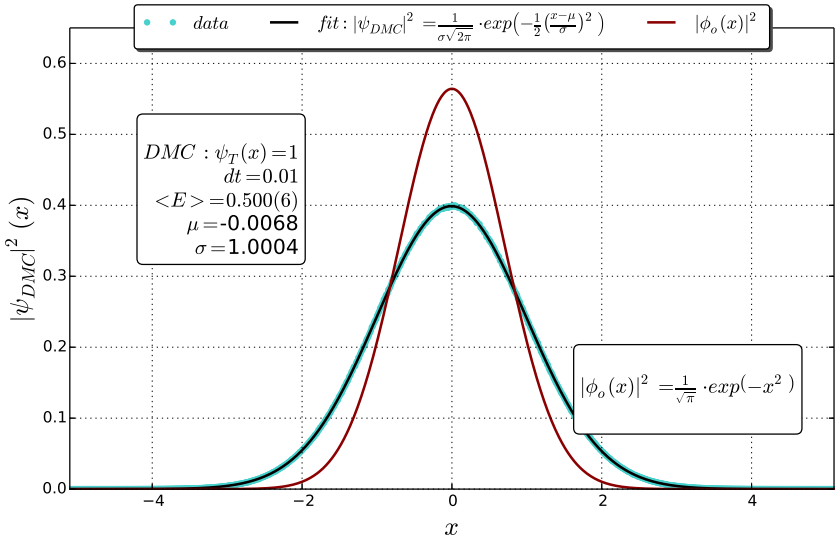

Figure A.1: Probability distribution of the QHC with and without guiding wave function.

The use of a trial wave function permits to sample the ground state function is more efficient. We report the dynamics of the DMC with a good guess for Ψ_T. In figure A2 we show how

the kinetic energy react to the variations of the potential and vice versa, helping to reduce the variance of the total energy.

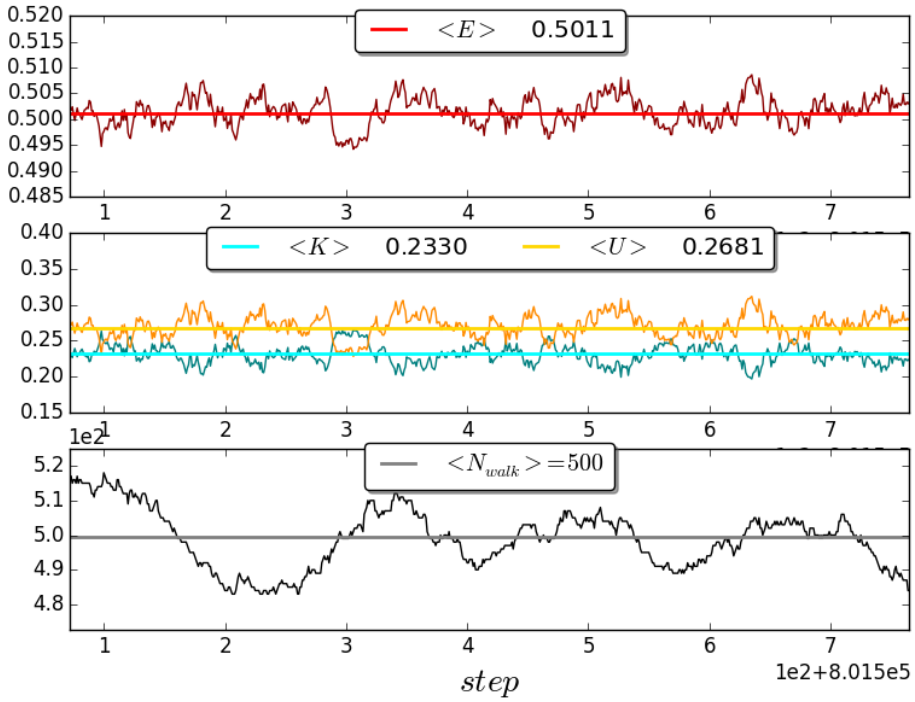

Figure A.2: Monitoring energy and walkers.

We can also see how the population evolves arround a mean value (in this case 500 walkers) in a 'natural' way, it is without abrupt changes. However, it is not odd to see abrupt changes once in a while due to the population control implemented.

Another characteristic of the energy that is generic, regardless the system under analysis, is the Gaussian shape of the energy distribution arround the mean value.

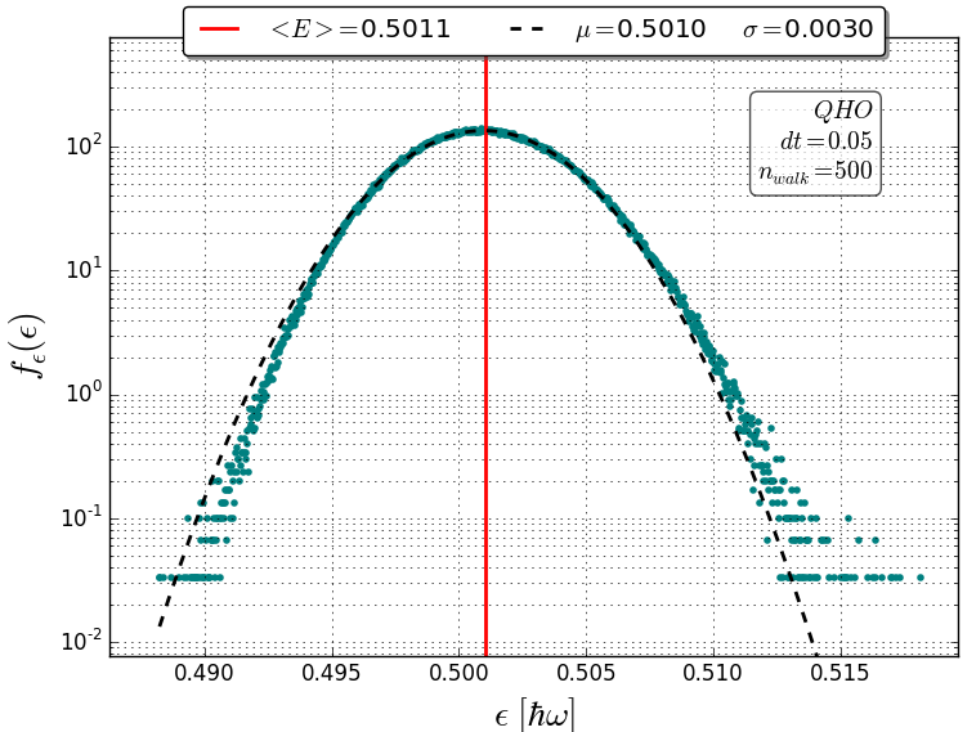

So the previous plot is a desirable shape for the energy distribution of a given system, and it will be better the better the variance will be.

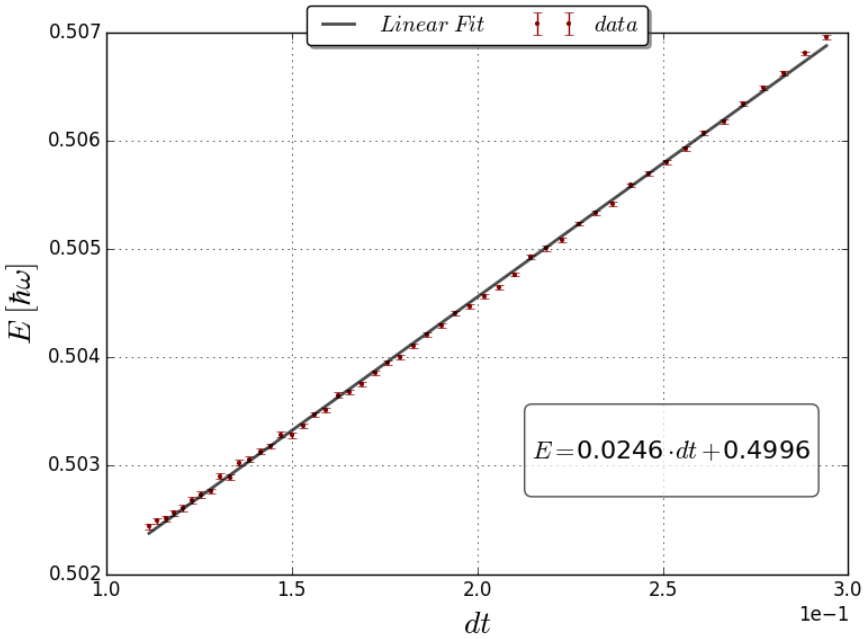

Another feature that has to be tested is the linear convergence of the g.s. energy in terms of the time step. In a well performed simulation, the energy given by the code evolves linearly with the time step (for a linear DMC), to a optimum value (it is the real value of the energy) when $dt \to 0$. It can be seen in the above figure, where the value of the energy fits well the theoretical result.

$$E = 0.0246 \cdot dt + 0.4996; \qquad E_0 = \lim_{dt \to 0} E = 0.4996 \tag{A.2}$$

It can also be verified that the energy variance decreases as the trial wave function is improved, arriving to be zero when the guide wave function is ϕ_0, since the energy here is indeed an eigenvalue of the Hamiltonian.

Bibliography

[1] M. H. Anderson, J. R. Ensher, M. R. Matthews, C. E. Wieman, and E. A. Cornell, "Observation of bose-einstein condensation in a dilute atomic vapor," *science*, vol. 269, no. 5221, pp. 198–201, 1995.

[2] S. Bose, "Planck's law and the hypothesis of light quanta," *Zeitschrift für Physik*, no. 26, pp. 178–181, 1924.

[3] A. Einstein, "Quantum theory of ideal monatomic gases," *Sitzber. Preuss. Akad. Wiss*, p. 261–267, 1924.

[4] A. Einstein, "Quantum theory of ideal monoatomic gases," *Sitzber. Preuss. Akad. Wiss*, vol. 23, no. 3, 1925.

[5] P. A. Dirac, "On the theory of quantum mechanics," in *Proceedings of the Royal Society of London A: Mathematical, Physical and Engineering Sciences*, vol. 112, pp. 661–677, The Royal Society, 1926.

[6] E. Fermi, "Sulla quantizzazione del gas perfetto monoatomico," *Rend. Lincei*, vol. 3, pp. 145–149, 1926.

[7] J. Klaers, J. Schmitt, F. Vewinger, and M. Weitz, "Bose-einstein condensation of photons in an optical microcavity," *Nature*, vol. 468, no. 7323, pp. 545–548, 2010.

[8] A. Leanhardt, T. Pasquini, M. Saba, A. Schirotzek, Y. Shin, D. Kielpinski, D. Pritchard, and W. Ketterle, "Cooling bose-einstein condensates below 500 picokelvin," *Science*, vol. 301, no. 5639, pp. 1513–1515, 2003.

[9] A. Görlitz, J. Vogels, A. Leanhardt, C. Raman, T. Gustavson, J. Abo-Shaeer, A. Chikkatur, S. Gupta, S. Inouye, T. Rosenband, *et al.*, "Realization of bose-einstein condensates in lower dimensions," *Physical Review Letters*, vol. 87, no. 13, p. 130402, 2001.

[10] M. Greiner, I. Bloch, O. Mandel, T. W. Hänsch, and T. Esslinger, "Exploring phase coherence in a 2d lattice of bose-einstein condensates," *Physical Review Letters*, vol. 87, no. 16, p. 160405, 2001.

[11] D. Rychtarik, B. Engeser, H.-C. Nägerl, and R. Grimm, "Two-dimensional bose-einstein condensate in an optical surface trap," *Physical review letters*, vol. 92, no. 17, p. 173003, 2004.

[12] V. Bagnato and D. Kleppner, "Bose-einstein condensation in low-dimensional traps," *Physical Review A*, vol. 44, no. 11, p. 7439, 1991.

[13] J. Luttinger, "An exactly soluble model of a many-fermion system," *Journal of Mathematical Physics*, vol. 4, no. 9, pp. 1154–1162, 1963.

[14] W. Kolos and L. Wolniewicz, "Improved theoretical ground-state energy of the hydrogen molecule," *The Journal of Chemical Physics*, vol. 49, no. 1, pp. 404–410, 1968.

[15] M. Jamieson, A. Dalgarno, and L. Wolniewicz, "Calculation of properties of two-center systems," *Physical Review A*, vol. 61, no. 4, p. 042705, 2000.

[16] L. V. Markić, J. Boronat, and J. Casulleras, "Quantum monte carlo simulation of spin-polarized h," *Physical Review B*, vol. 75, no. 6, p. 064506, 2007.

[17] I. Bešlić, L. V. Markić, and J. Boronat, "Spin-polarized hydrogen and its isotopes: A rich class of quantum phases (review article)," *Low Temperature Physics*, vol. 39, no. 10, pp. 857–873, 2013.

[18] I. Bešlić, L. V. Markić, and J. Boronat, "Quantum monte carlo study of large spin-polarized tritium clusters," *The Journal of chemical physics*, vol. 131, no. 24, p. 244506, 2009.

[19] H. Xu and J.-P. Hansen, "Structural and thermodynamic properties of spin-polarized fluid hydrogen," *Physics of Plasmas (1994-present)*, vol. 9, no. 1, pp. 21–27, 2002.

[20] I. Bešlić, L. V. Markić, J. Casulleras, and J. Boronat, "Quantum monte carlo study of spin-polarized deuterium," *Physical Review B*, vol. 88, no. 2, p. 024507, 2013.

[21] G. Astrakharchik and J. Boronat, "Luttinger-liquid behavior of one-dimensional he 3," *Physical Review B*, vol. 90, no. 23, p. 235439, 2014.

[22] M. Boninsegni, "Ground state phase diagram of parahydrogen in one dimension," *Physical review letters*, vol. 111, no. 23, p. 235303, 2013.

[23] R. Guardiola, *Monte Carlo techniques in the many body problem*. Departament of Nuclear Physics, University of Granada.

[24] G. Astrakharchik, J. Boronat, J. Casulleras, and S. Giorgini, "Beyond the tonks-girardeau gas: Strongly correlated regime in quasi-one-dimensional bose gases," *Physical review letters*, vol. 95, no. 19, p. 190407, 2005.

[25] M. Girardeau, "Relationship between systems of impenetrable bosons and fermions in one dimension," *Journal of Mathematical Physics*, vol. 1, no. 6, pp. 516–523, 1960.

[26] D. K.Binder, *Monte Carlo Simulation in Statistical Physics*. Springer.

[27] M. Cazalilla, "Bosonizing one-dimensional cold atomic gases," *Journal of Physics B: Atomic, Molecular and Optical Physics*, vol. 37, no. 7, p. S1, 2004.